# Upscale Impact of Mesoscale Disturbances of Tropical Convection on Synoptic-Scale Equatorial Waves in Two-Dimensional Flows

Qiu Yang* and Andrew J. Majda

*Department of Mathematics and Center for Atmosphere Ocean Science, Courant Institute of Mathematical Sciences, New York University, New York, NY, USA*

**Corresponding author address:* Qiu Yang, Courant Institute of Mathematical Sciences, New York University, 251 Mercer Street, New York, NY, 10012

E-mail: yangq@cims.nyu.edu

ABSTRACT

Superclusters of cloudiness on the synoptic scale are frequently organized by convectively coupled equatorial waves (CCEWs). Within the large-scale convective envelope, numerous mesoscale disturbances of tropical convection are typically found. It is a challenge for present-day numerical models to simulate such multi-scale structure of tropical convection. Also, the upscale impact of mesoscale disturbances on the behavior of synoptic-scale circulation is unclear. It is still not well understood how much of synoptic-scale circulation is induced by upscale impact of mesoscale disturbances instead of mean heating. Here a simple two-dimensional multi-scale model for scale interactions across mesoscale and synoptic scale is used. A prescribed two-scale heating drives synoptic-scale circulation through eastward-moving mean heating and eddy transfer of momentum and temperature, where the latter represents the upscale impact of mesoscale disturbances driven by westward-moving mesoscale heating. This multi-scale model successfully reproduces many key features of flow fields with a front-to-rear tilt, which are compared with results from a cloud resolving model. In the scenario with an elevated upright mean heating, the tilted vertical structure of synoptic-scale circulation is still induced from the upscale impact of mesoscale disturbances. In the faster propagation scenario, the upscale impact becomes less important due to competing effects of eddy transfer of momentum and temperature, while the synoptic-scale circulation response to mean heating dominates, in agreement with cloud resolving models. In the unrealistic scenario with upward/westward tilted mesoscale heating, positive potential temperature anomalies are induced in the leading edge, which will suppress shallow convection in a moist environment.

## 1. Introduction

Tropical convection is organized in a hierarchy of multiple spatial and temporal scales, ranging from cumulus clouds over several kilometers to mesoscale circulation systems (MCSs) (Houze 2004) to CCEWs (Kiladis et al. 2009) to intraseasonal oscillations on the planetary scale such as the Madden-Julian Oscillation (MJO) (Zhang 2005). The early investigation about mean properties of tropical convection and its variability based on the GARP Atlantic Tropical Experiment (GATE) dates back to 1970s (Houze Jr and Cheng 1977). Recently, organized tropical convection is documented in the Year of Tropical Convection (YOTC) virtual global field-campaign and further analyzed through diagnostic, theoretical and numerical studies (Moncrieff et al. 2012). In particular, superclusters of cloudiness and rainfall on the synoptic scale are frequently organized by CCEWs that propagates eastward or westward along the equator or the intertropical Convergence Zone (ITCZ) (Nakazawa 1988; Kiladis et al. 2009). For example, cloudiness variations associated with convectively coupled Kelvin waves have a peak along the latitude of the climatological ITCZ, indicating significant variability of convective activities (Wheeler et al. 2000; Kiladis et al. 2009). The crucial impacts of convectively coupled Kelvin waves lie in their strong interaction with the MJO (Straub et al. 2006) and linking synoptic-scale variation of the Atlantic ITCZ with precipitation anomalies in South America (Wang and Fu 2007). Instead of organizing in a single-scale convective envelope, CCEWs are manifested in a hierarchical structure where numerous mesoscale convective elements are embedded in the synoptic-scale convective envelope. The examples of CCEWs in such a multi-scale structure include the convectively coupled Kelvin wave observed in the eastern Pacific ITCZ where many small-scale, westward-moving convective elements over several hundred kilometers are found in the large-scale convective envelope (Straub and Kiladis 2002), and the 2-day wave observed over the Indo-Pacific oceanic warm pool where numerous embedded cloud clusters propagate at various speeds and directions (Chen et al. 1996). These small-scale convective elements are categorized as MCSs, which are the dominant heavy rain producers in the tropics and subtropics, providing more than 50% of the precipitation (Tao and Moncrieff 2009).

The morphology of organized tropical convection is similar across multiple scales from the mesoscale to synoptic scale to planetary scale, which is explained by a self-similarity principle derived by Majda (2007). One crucial feature of self-similarity is that both dynamical and convective fields during tropical convection exhibit a front-to-rear vertical tilt. By regarding an MCS as a small analogue or prototype of large-scale waves, the self-similarity of cloudiness is explained as a similar progression from shallow to deep convection to stratiform anvils on many time scales (Mapes et al. 2006). Such a trimodal characteristics of tropical convection including cumulus congestus, deep convection and stratiform clouds is also found in a broad spectrum based on shipboard radar data (Johnson et al. 1999). By parameterizing these three cloud types (congestus, deep, stratiform) and carefully dealing with the transition between different type clouds, the multicloud models successfully reproduce many key features of CCEWs including the spectrum peaks, reduced phase speed and self-similar front-to-rear tilt (Khouider and Majda 2008a). Besides, the large-scale organization of tropical deep convection is investigated in idealized two-dimensional cloud-resolving simulations (Grabowski and Moncrieff 2001). Their results highlight westward-moving MCSs over several hundred kilometers embedded in an eastward-moving convective envelope over several thousand kilometers.

Understanding the scale interaction between small-scale disturbances and large-scale wave envelope is crucial, not only for explaining propagation properties and spatial patterns of CCEWs, but also improving the skill of global climate models (GCMs) for weather and climate forecasting. Based on soundings, the momentum budget residual is estimated for the effects of convective momentum transport (CMT) over the western Pacific warm pool (Tung and Yanai 2002a,b). In general, CMT not only describes the momentum transport when organized moist convection on smaller scales affects the large-scale flow field, but also involves the process of energy conversion from convective available potential energy to horizontal kinetic energy. In the theoretical directions, simple stochastic models that capture the significant intermittent upscale impact of CMT on the large scales due to organized unresolved convection from squall lines are built and further tested in the column model environment and the organized synoptic-scale CCEWs through an idealized multicloud model (Majda and Stechmann 2008). Besides, a simple dynamic model is derived by including interactions between a large-scale zonal mean flow and convectively coupled gravity waves and utilized to quantify and parameterize the effects of CMT (Majda and Stechmann 2009). Furthermore, CMT and its impact on the large-scale organization of convection are diagnostically investigated in the two-dimensional cloud-resolving model (Grabowski and Moncrieff 2001) and three-dimensional state-of-the-art mesoscale model (Khouider and Han 2013).

In spite of so much progress, the crucial features of the MCSs and their upscale impact on the large-scale circulation and precipitation are still poorly simulated in the GCMs, which is mainly related with the fact that the resolution of GCMs is too coarse to explicitly simulate the dynamical and thermal properties of MCSs. In addition, there still exist huge discrepancies of precipitation amounts between the comprehensive numerical simulations and the observed tropical convection. For example, the present-day GCMs are still struggling to reproduce the realistic features of the MJO (Jiang et al. 2015). One hypothesis for such huge discrepancies of precipitation amount is the inadequate treatment of organized tropical convection and its missing upscale impact on the large-scale flow field in the GCMs. The goals of this paper are as follows: first, using a simple multi-scale model to capture the hierarchical structure of synoptic-scale equatorial waves with westward-moving mesoscale systems embedded in a eastward-moving synoptic-scale convective envelope;

secondly, assessing the upscale impact of mesoscale disturbances on the behaviors of synoptic-scale circulation through eddy transfer of momentum and temperature; thirdly, understanding how much of synoptic-scale circulation is induced by eddy transfer of momentum and temperature rather than synoptic-scale mean heating.

The simple multi-scale model used in this paper is the mesoscale equatorial synoptic dynamics (MESD) model, originally derived by Majda (2007). In general, self-consistent multi-scale models such as the MESD model were derived systematically by following multi-scale asymptotic theory and used to describe the hierarchical structures of atmospheric flows in the tropics (Majda and Klein 2003; Majda 2007; Yang and Majda 2014; Majda and Yang 2016). The advantages of using these multi-scale models lie in isolating the essential components of multi-scale interaction and providing assessment of the upscale impact of the small-scale fluctuations onto the large-scale envelope through eddy flux divergence of momentum and temperature in a transparent fashion. Specifically, the MESD model can be used to model the cluster-supercluster interactions across mesoscale and synoptic scale and incorporate them together in a simple multi-scale framework.

In order to achieve the goals mentioned before, the two-dimensional MESD model is first set up in the same manner as the two-dimensional cloud-resolving model (Grabowski and Moncrieff 2001). The resulting MESD model solutions are directly compared with those figures in (Grabowski and Moncrieff 2001) in terms of zonal momentum, vertical velocity and potential temperature anomalies. Then three different scenarios are discussed, where synoptic-scale circulation is driven by various two-scale heating including elevated upright mean heating, faster propagating convective envelope and westward-moving mesoscale heating in an upward/westward tilt. Several crucial results are obtained by calculating eddy transfer of momentum and temperature and comparing synoptic-scale circulation response to mean heating and eddy terms. First, the two-dimensional MESD model successfully reproduces many key features of flow fields, including the front-to-rear tilted vertical structure of mesoscale systems, and synoptic-scale circulation. Secondly, in the scenario with an upright mean heating, the total potential temperature anomalies and zonal velocity still have front-to-rear tilted vertical structure, highlighting the significant upscale impact of the mesoscale disturbances on the spatial pattern of synoptic-scale circulation. Thirdly, in the scenario with a faster propagating convective envelope (less than 25 $ms^{-1}$), the MESD model predicts that the synoptic-scale circulation response to the eddy terms become less important due to the competing effects of eddy transfer of momentum and temperature, while that driven by mean heating dominates. Such a result can explain the discrepancies between the cloud resolving simulations in trade wind regime by Grabowski and Moncrieff (2001) where CMT is significant and those in zero background mean flow regime by Tulich and Mapes (2008) where CMT is negligible. Lastly, in the scenario with westward-moving mesoscale heating in an upward/westward tilt, positive potential temperature anomalies are induced by eddy terms in the leading edge of the convective envelope, which tends to suppress shallow convection in a moist environment.

The rest of this paper is organized as follows. Sec.2 summarizes the properties of the two-dimensional MESD model and self-similarity of flow field across mesoscale and synoptic scale. Sec.3 discusses the prescribed westward-moving mesoscale heating, mesoscale fluctuations of flow field and the associated eddy transfer of momentum and temperature. Sec.4 shows synoptic-scale circulation response to the eastward-moving mean heating with embedded westward-moving mesoscale heating, which are directly compared with the results from the cloud-resolving model (Grabowski and Moncrieff 2001). Sec.5-7 consider three different scenarios with elevated upright mean heating, faster propagating convective envelope and westward-moving mesoscale heating in an upward/westward tilt. The paper ends with a concluding discussion. A proof about zero upscale fluxes from free gravity waves is included in the Appendix.

## 2. Properties of the MESD Model

One common feature of CCEWs in the tropics is that numerous smaller-scale convective elements are embedded in the large-scale convective envelope (Straub and Kiladis 2002; Chen et al. 1996), which is a suitable scenario for using the multi-scale models. In general, the multispace, multitime simplified asymptotic models are derived systematically from the equatorial primitive equations on an equatorial $\beta$-plane, providing a useful framework to understand the multi-scale phenomenon (Majda and Klein 2003; Majda 2007). Particularly, the three-dimensional MESD model originally derived by Majda (2007) consists of two groups of linear primitive equations, one of which governs irrotational mesoscale flows with gravity waves and the other one of which governs rotational synoptic-scale flows with baroclinic Kelvin waves, Rossby waves, mixed Rossby-gravity waves, gravity waves and barotropic Rossby waves (Majda 2003). More importantly, eddy transfer terms involving mesoscale fluctuations of momentum and temperature arise naturally in the synoptic-scale equations and drive the synoptic-scale circulation response along with mean heating, where the former is interpreted as the upscale impact of mesoscale disturbances on the synoptic-scale circulation.

### *a. The two-dimensional MESD model*

Rather than the original three-dimensional MESD model (Majda 2007), the two-dimensional MESD model is used in this paper. Such a simplified version of MESD model can not only simplify our discussion, but provide a suitable scenario to have direct comparison with the two-dimensional cloud resolving model (Grabowski and Moncrieff 2001). In fact, it is quite straightforward to achieve such dimensionality reduction by just assuming that the dominant flow field is near the equator (the Coriolis force is negligible) and meridionally symmetric (meridional velocity and meridional momentum forcing vanishes). The resulting two-dimensional MESD model consists of two groups of equations on mesoscale and synoptic scale respectively.

The **equations for mesoscale dynamics** in dimensionless units read as follows,

$$u'_\tau = -p'_x + s'_u, \tag{1a}$$

$$\theta'_\tau + w' = s'_\theta, \tag{1b}$$

$$p'_z = \theta', \tag{1c}$$

$$u'_x + w'_z = 0, \tag{1d}$$

where the prime means mesoscale fluctuations of flow fields. $s'_u$ and $s'_\theta$ stand for momentum and thermal forcing on the mesoscale.

The **equations for synoptic-scale dynamics** in dimensionless units read as follows,

$$U_t = -P_X - dU - \left\langle \overline{w'u'} \right\rangle_z + \left\langle \bar{S}^u \right\rangle, \tag{2a}$$

$$\Theta_t + W = -d_\theta \Theta - \left\langle \overline{w'\theta'} \right\rangle_z + \left\langle \bar{S}^\theta \right\rangle, \tag{2b}$$

$$P_z = \Theta, \tag{2c}$$

$$U_X + W_z = 0, \tag{2d}$$

where $\left\langle \bar{S}^u \right\rangle$ and $\left\langle \bar{S}^\theta \right\rangle$ stand for momentum and thermal forcing on the synoptic scale.

A linear momentum damping term is added in Eqs.2a to mimic momentum dissipation of cumulus drag. The coefficient $d$ in units of $1/day$ sets the time scale for momentum dissipation. According to the observation, momentum damping time scale at the surface of the Pacific ocean could be as strong as 1 day (Deser 1993) while that at the upper troposphere is much longer. In general, the momentum damping of large-scale circulation occurs on a time scale of $\mathscr{O}(1-10)$ days, and also depends on the vertical wavelength of the wind profile (Romps 2014). Besides, the Newtonian cooling term $-d_\theta \Theta$ is added in the thermal equation in Eq.2b to mimic radiative cooling. Such thermal damping in two-dimensional MESD model is necessary, otherwise potential temperature anomalies induced by heating forcing in Eq.2b grows linearly to infinity.

The two-dimensional MESD model describes hierarchical structure of tropical flows across multiple spatial and temporal scales. One dimensionless unit of $x$, $\tau$ corresponds to 150 $km$, 50 $min$ on the mesoscale, while that of $X$, $t$ corresponds to 1500 $km$ and 8.3 $h$ on the synoptic scale. On these two scales, one dimensionless unit of some physical variables corresponds to the same dimensional value, including zonal velocity $u,U$ (5 $ms^{-1}$), pressure perturbation $p,P$ (250 $m^2s^{-2}$), potential temperature anomalies $\theta,\Theta$ (3.3 $K$). In contrast, vertical velocity in one dimensionless value corresponds to 0.16 $ms^{-1}$ one the mesoscale and 0.016 $ms^{-1}$ on the synoptic scale. The vertical coordinate $z$ is shared by groups of equations on different scales. Furthermore, the momentum and thermal forcing on the synoptic scale is much weaker than those on the mesoscale by one order, which is consistent with the observation that the measured atmospheric heating from latent heat release in the tropics is in general much weaker on synoptic and even larger scales (Biello and Majda 2010). More details for all constants and physical parameters are summarized in Table.1.

Eqs.2a-2d involve mesoscale zonal and temporal averaging operators defined as follows ($f$ is an arbitrary function),

$$\bar{f}(X,z,t,\tau) = \lim_{L\to\infty} \frac{1}{2L_x} \int_{-L_x}^{L_x} f(X,x,z,t,\tau)\, dx \tag{3}$$

$$\langle f \rangle (X,x,z,t) = \lim_{T\to\infty} \frac{1}{2T} \int_{-T}^{T} f(X,x,z,t,\tau)\, d\tau \tag{4}$$

where $L_x$ is the mesoscale zonal length of the domain and $T$ is the time range in the asymptotic limit. In Eqs.1a-1d, all mesoscale physical variables $f'$ satisfy $\bar{f}' = 0$ and $\langle f' \rangle = 0$, representing mesoscale fluctuations of flow fields.

### *b. Self-similarity of flow fields across mesoscale and synoptic scale*

The governing equations for mesoscale dynamics in Eqs.1a-1d and synoptic-scale dynamics in Eqs.2a-2d have many features in common. Specifically, if the momentum damping term $-dU$, radiative cooling term $-d_\theta\Theta$ and all eddy terms $-\left\langle\overline{w'u'}\right\rangle_z$, $-\left\langle\overline{w'\theta'}\right\rangle_z$ are merged into the general forcing terms on the right hand side, the mesoscale dynamics in Eqs.1a-1d are exactly the same as the synoptic-scale dynamics in Eqs.2a-2d. Such self-similarity principle is derived by Majda (2007).

With rigid-lid boundary conditions imposed, the governing equations in common across mesoscale and synoptic scale have explicit solution formulas involving the barotropic mode and an infinite set of baroclinic modes (Majda 2003). For vertical decomposition, all physical variables are expanded into different vertical modes with sine and cosine functions as follows,

$$f = \sum_{q=0}^{\infty} f_q \cos(qz), \; f \in \{u, p, s^u\} \tag{5}$$

$$g = \sum_{q=1}^{\infty} g_q \left[-q\sin(qz)\right], \; g \in \left\{\theta, w, s^\theta\right\} \tag{6}$$

where $q$ is the index for different vertical modes. The barotropic mode in Eq.6 vanishes due to the rigid-lid boundary condition.

After plugging all physical variables into the ansatz in Eqs.5-6, the governing equations are decomposed into different groups of equations in barotropic and baroclinic modes. The barotropic mode ($q = 0$) is governed by the following equations,

$$u_t = -p_x + s^u \tag{7a}$$

$$u_x = 0 \tag{7b}$$

which states that the time tendency of mean zonal velocity $\bar{u}_t$ is only forced by mean zonal momentum forcing $\bar{s}^u$, while nonzero wavenumber mode of zonal velocity vanishes and that of pressure gradient $p_x$ is balanced by zonal momentum forcing $s^u$.

The baroclinic mode ($q \neq 0$) is governed by the following equations,

$$u_t = -p_x + s^u \tag{8a}$$

$$\theta_t + w = s^\theta \tag{8b}$$

$$p = \theta \tag{8c}$$

$$u_x - q^2 w = 0 \tag{8d}$$

where $q$ is the vertical index. The subscripts and superscripts of physical variables are ignored for simplicity. After plugging in the plane wave ansatz, the dispersion relation of gravity waves is obtained,

$$\omega = \pm\frac{k}{q} \tag{9}$$

which indicates that the phase speed in the $q$ baroclinic mode is $c = \frac{\omega}{k} = \pm\frac{1}{q}$ in both eastward and westward directions. Also, gravity waves in higher baroclinic modes propagate slower. For example, in dimensional units, the phase speeds of gravity waves in the 1st, 2nd and 3rd baroclinic modes are 50 $ms^{-1}$, 25 $ms^{-1}$ and 16.7 $ms^{-1}$.

## 3. Westward-Moving Mesoscale Disturbances and the Upscale Flux

Inside the convective envelope of synoptic-scale waves, numerous convective elements on the smaller scales are found, which is associated with MCSs such as squall-line systems (Houze Jr 1975, 1977; Houze Jr and Cheng 1977; Houze 2004). Such hierarchical structure of the synoptic-scale convective envelope with embedded MCSs is captured in an idealized two-dimensional cloud resolving simulations (Grabowski and Moncrieff 2001). Within the large-scale organization of convection, numerous westward-moving systems are identified, which are characterized by low-level inflow and upper-level outflow to both east and west with extensive stratiform cloud in the upper troposphere.

The main goal of this section is to model such mesoscale convective systems by using the mesoscale dynamics equations in Eqs.1a-1d and prescribing top-heavy diabatic heating to mimic latent heat release. In the vertical direction, the rigid-lid boundary conditions are imposed,

$$w = 0, \text{ at} z = 0, \pi. \tag{10}$$

where $z = 0, \pi$ denote the surface and the top of troposphere. The mesoscale solutions are assumed to be periodic in the zonal direction. The vertical extent of the domain is 15.7 *km*. Since it is proved in the Appendix that free gravity waves on the mesoscale can not generate upscale fluxes, here the mesoscale solutions forced by prescribed heating are solved analytically and all free gravity waves are ignored.

### *a. Westward-moving mesoscale heating*

In order to mimic latent heat release from westward-moving systems with extensive stratiform clouds in the upper troposphere in (Grabowski and Moncrieff 2001), a top-heavy mesoscale heating is prescribed below,

$$s'_\theta = c_0 \left[\sin(kx + \omega\tau)\sin(z) + \alpha \sin(kx + \omega\tau + \phi_0)\sin(2z)\right] \tag{11}$$

where the magnitude coefficient is $c_0 = 0.7$ in dimensional unit 100 $Kday^{-1}$. The wavenumber $k = \frac{3\pi}{5}$ is chosen for wavelength 500km, qualitatively consistent with typical length scales of MCSs (Houze 2004). The frequency $\omega = \frac{12}{50}k$ is picked so that the associated phase speed reaches 12 $ms^{-1}$, the same as the averaged westward propagation speed of mesoscale systems in (Grabowski and Moncrieff 2001). The strength coefficient of the second baroclinic mode $\alpha$ is set as -0.9 to obtain top-heavy heating profile. The phase lag $\phi_0 = -\pi/4$ between the first and second baroclinic modes is used to mimic the upward/eastward tilted heating.

Fig.1 shows the prescribed mesoscale heating profile in the longitude-height diagram. Such a mesoscale heating in a front-to-rear tilt is frequently observed in MCSs (Houze Jr 1977; Houze 2004). Meanwhile, heating and cooling regions reach their maximum magnitudes about $100 K day^{-1}$ in the upper troposphere at the height 11.5 *km*. In fact, heating profiles with the first baroclinic mode for deep convective heating and the second baroclinic mode for both congestus and stratiform heating have been utilized successfully in the multicloud models to reproduce many realistic features of tropical convection (Khouider and Majda 2006b,a, 2007).

### *b. Mesoscale fluctuations of zonal velocity and potential temperature anomalies*

Fig.2a shows the solution of zonal velocity in the longitude-height diagram, which is directly compared with Fig.2b from the study (Grabowski and Moncrieff 2001). These two panels are qualitatively similar to each other and both feature zonal velocity in a front-to-rear tilt. In details, zonal velocity in this westward-moving mesoscale system is characterized by an inflow layer of westerly winds, which starts from the lower levels to the west, lifts up to the middle troposphere in the middle of the domain and continuously extends to the upper troposphere to the east. The maximum magnitude of westerly winds is reached in the upper troposphere to the east. Besides, there are low-level easterly winds to the east and upper-level easterly winds to the west. Fig.2c shows the stream lines of mesoscale flow fields. When compared with Fig.2d from the study (Grabowski and Moncrieff 2001), both panels are characterized by wind convergence in the lower troposphere and wind divergence in the upper troposphere in a front-to-rear tilt.

Fig.2e shows potential temperature anomalies in the longitude-height diagram. In the vertical direction, potential temperature anomalies are mostly characterized by opposite anomalies between upper and lower tropospheres, indicating the significant magnitude of the second baroclinic mode. Fig.2f shows vertical velocity in the longitude-height diagram, whose spatial pattern is quite similar to that of mesoscale heating. In connection with mesoscale heating in Fig.1, heating regions are dominated by the westward/downward winds while cooling regions are dominated by the eastward/upward winds.

### *c. Eddy transfer of momentum and temperature*

In the MESD model, the governing equations for synoptic-scale dynamics is forced by two eddy terms on the right hand side in Eq.2a-2b. By utilizing the mesoscale solutions of zonal and vertical velocity, eddy momentum transfer (EMT) has the following expression,

$$
\begin{aligned}
F^u &= -\left\langle \overline{w'u'} \right\rangle_z \\
&= \kappa^u \left[ -\frac{3}{2}\cos(z) + \frac{3}{2}\cos(3z) \right]
\end{aligned}
\tag{12}
$$

which represents upscale impact of mesoscale disturbances on the synoptic-scale circulation in the zonal momentum budget. In fact, EMT is referred as CMT, which has been studied from different perspectives to highlight its significance such as stochastic models (Majda and Stechmann 2008; Khouider et al. 2012) and dynamical models with cloud parameterization (Majda and Stechmann 2009). Physically, positive (negative) anomalies of EMT corresponds to eastward (westward) momentum forcing on the synoptic-scale circulation. One crucial feature of the EMT term is that its vertical profile is independent of all the parameters, while its magnitude and directions are determined by the coefficient $\kappa^u$ in the following explicit expression,

$$
\kappa^u = \frac{\sin(\phi_0)\,\alpha k^3}{2(\omega^2 - k^2)(4\omega^2 - k^2)}. \tag{13}
$$

Since the product term $\sin(\phi_0)\alpha$ controls the vertical structure of mesoscale heating in Eq.11, its tilting direction (upward/eastward or upward/westward) determines the sign of EMT. Besides, there exist two critical phase speeds of mesoscale heating $|\frac{\omega}{k}| = 1, 0.5$, which actually corresponds to those of the first and second baroclinic modes as discussed in Sec.2b.

Fig.3a shows the vertical profile of eddy fluxes of zonal momentum and EMT. The eddy fluxes of zonal momentum reaches its maximum positive value in the middle troposphere and decays to zero in both the upper and lower boundaries, due to the in-phase relation between zonal velocity and vertical velocity as shown in Fig.2. The EMT term is characterized by its positive anomalies in the upper troposphere near the height 11 *km* and negative anomalies in the lower troposphere near the height 5 *km*. Such upper-level eastward momentum forcing and low-level westward momentum forcing represent vertical transfer of zonal momentum on the synoptic scale, resulting in vertical shear of zonal winds.

The other eddy term that appears at the right hand side of the synoptic-scale equations is eddy heat transfer (EHT). By utilizing the mesoscale solutions of vertical velocity and potential temperature anomalies, its expression is as follows,

$$\begin{aligned} F^{\theta} &= -\left\langle \overline{w'\theta'} \right\rangle_z \\ &= \kappa^{\theta} \left[ -\frac{3}{2}\sin(z) + \frac{9}{2}\sin(3z) \right] \end{aligned} \tag{14}$$

which represents upscale impact of mesoscale disturbances on the synoptic-scale thermal dynamics. Physically, positive (negative) anomalies of EHT corresponds to heating (cooling) on the synoptic-scale circulation. The coefficient $\kappa^{\theta}$,

$$\kappa^{\theta} = \frac{\sin(\phi_0)\,\alpha k^2 \omega}{2(\omega^2 - k^2)(4\omega^2 - k^2)}. \tag{15}$$

which is quite similar to that in Eq.13 except that wavenumber $k$ in the numerator is replaced by frequency $\omega$. Suppose wavenumber $k$ is fixed, the sign of frequency $\omega$ determines the propagation direction of mesoscale heating. The product term $\sin(\phi_0)\alpha$ determines the front-to-rear tilted vertical structure. Therefore, the sign of EHT is determined by the tilting direction of mesoscale heating, compared with its propagation direction.

Fig.3b shows the vertical structure of eddy fluxes of temperature and EHT. The eddy fluxes of temperature reaches positive value in the upper troposphere near the height 11 *km* and negative value in the lower troposphere near the height 5 *km*, due to the opposite phase relation between potential temperature anomalies and vertical velocity in upper and lower tropospheres as shown in Fig.2. The EHT term is characterized by heating in both the lower and upper troposphere and cooling in the middle troposphere. In a moist environment, the heating in the lower troposphere could suppress the convection through increasing saturation rate of vapor and convective inhibition.

The ratio between EMT and EHT in dimensionless units determines relative strength of the corresponding synoptic-scale circulation response. In fact, the ratio between the magnitude coefficients $\kappa^u$ and $\kappa^\theta$ is equal to,

$$\frac{\kappa^\theta}{\kappa^u} = \frac{\omega}{k}, \tag{16}$$

which is equal to the phase speed of mesoscale heating and suggests that the strength of the corresponding circulation response to EMT and EHT depends on the propagation speed of the diabatic heating. Suppose the propagation speed of the diabatic heating is relatively slow, the synoptic-scale circulation response due to the upscale impact of mesoscale disturbances is mostly induced by the EMT. While in the fast propagating mesoscale heating scenario, the synoptic-scale circulation response is mostly induced by the EHT.

## 4. Synoptic-Scale Circulation Response to Upscale Impact of Mesoscale Disturbances and Mean Heating

The hierarchical structure of tropical convection has been identified by Nakazawa (1988) and further explained as a synoptic-scale eastward-moving convective envelope in a supercluster embedded by mesoscale westward-moving disturbances in cloud clusters. As discussed in Sec.3, mesoscale fluctuations in tilted vertical structure tend to generate eddy transfer of momentum and temperature and drive synoptic-scale circulation response. In this section, the synoptic-scale circulation response induced by upscale impact of mesoscale disturbances and mean heating is directly compared with results from the study (Grabowski and Moncrieff 2001).

Here the equations for synoptic-scale dynamics in Eqs.2a-2d are used. By ignoring the synoptic-scale momentum forcing in Eq.2a, the synoptic-scale circulation response is driven by mean heating , EMT and EHT. As for boundary conditions, the solutions are assumed to be periodic in the zonal direction. In the vertical direction, rigid-lid boundary conditions are imposed,

$$W = 0, \,\mathrm{at}\, z = 0, \pi \tag{17}$$

where $z = 0, \pi$ stand for surface and top of the troposphere. The full domain is $0 \leq x < 20,000km$, $0 \leq z \leq 15.7km$. As for the damping terms, the momentum damping coefficient $d = d(z)$ is assumed to be a linear function of height, which contains 16.6 $h$ damping time scale at surface and 2.9 $day$ damping time scale at top of the troposphere. The radiative cooling coefficient $d_\theta = 0.1572$ (2.2 $day$) is assumed to be homogeneous throughout the whole domain, similar to (Grabowski and Moncrieff 2001). All physical variables are initialized from a state of rest and run for 41.5 $day$. The details for spatial and temporal resolutions are summarized in Table.2.

Tropical cloud clusters within the superclusters are found to experience different life stages from the developing to the east of the convective envelope to the mature stage in the middle to the decaying stage to the west (Nakazawa 1988). The large-scale modulation of the mesoscale fluctuations is represented by a synoptic-scale envelope function below,

$$E(X - st) = 0.5 + 0.5 \sin\left(\frac{10\pi}{L}(X - st)\right) \tag{18}$$

where $s = \frac{4}{25}$ (corresponds to 8 $ms^{-1}$) is the propagation speed of the envelope. $L = 40/3$ (20,000km) is the zonal extent of the whole domain. The envelope function has 5 complete periods throughout the whole domain, the same as (Grabowski and Moncrieff 2001). The mesoscale heating in a synoptic-scale convective envelope is reformulated as follows,

$$s'_\theta = E(X - st)\, c_0 \left[\sin(kx + \omega\tau)\sin(z) + \alpha \sin(kx + \omega\tau + \phi_0)\sin(2z)\right], \tag{19}$$

where all the parameters for the mesoscale heating are the same as Eq.11.

### a. Domain-averaged zonal velocity

According to Eq.2a, the domain-averaged zonal velocity is governed by,

$$\frac{\partial}{\partial t}\overline{U} = -d\overline{U} + \overline{F^u}, \tag{20}$$

where the long bar denotes zonal averaging about synoptic-scale $X$. Eq.20 indicates that the domain-averaged zonal velocity is only related with momentum damping coefficient $d$ and EMT $F^u$, while independent of EHT $F^\theta$ and mean heating $\langle \bar{S}^\theta \rangle$. In order to discuss domain-averaged zonal velocity, we only need to consider synoptic-scale circulation response to EMT.

The momentum flux $w'u'$ describes vertical transport of zonal momentum on the synoptic scale. As shown by Fig.4b, the momentum flux in the study (Grabowski and Moncrieff 2001) is characterized by five nearly equally spaced anomalies with their maximum value in the middle troposphere. Such mid-level momentum fluxes are captured in the numerical solutions in Fig.4a. According to Fig.3a, momentum fluxes reach their maximum value in the middle troposphere, which is consistent with the in-phase zonal and vertical velocity fields in Sec.3. Here the maximum magnitude of momentum fluxes is 0.18 $m^2 s^{-2}$, which qualitatively matches that in the study (Grabowski and Moncrieff 2001). As modulated by the envelope function in Eq.18, the momentum flux also has five positive anomalies along the whole domain.

Fig.4 shows zonal velocity induced by EMT in the longitude-height diagram at 41.5 $day$. The vertical profile of zonal velocity is characterized by low-level easterly winds at the height $z = 5km$ and upper-level westerly winds at the height $z = 11km$. Such vertical shear of zonal winds is consistent with that of EMT in Fig.3a. Due to the vertically decaying momentum damping coefficient, the maximum strength of zonal velocity in the upper troposphere is double as much as that in the lower troposphere. Near the surface and top of the troposphere, there are alternate easterlies and westerlies in weak magnitude. As shown by Fig.4e, the domain-averaged zonal velocity in the study (Grabowski and Moncrieff 2001) is characterized by strong westerly winds ($2ms^{-1}$) in the upper troposphere and relatively weak easterly winds ($1ms^{-1}$) in the lower troposphere. Such vertical shear of zonal velocity and comparable magnitude is captured in the MESD model numerical solutions as shown in Fig.4d. According to Eq.20, in the steady state, EMT is balanced by the zonal momentum damping, resulting in a vertical shear of zonal velocity. Such wind shear has been recognized to play a critical role for tropical convection and its organization (Grabowski et al. 1996; Grabowski and Moncrieff 2001).

### *b. Potential temperature anomalies on the synoptic scale*

The spatial distribution of temperature perturbations in the study (Grabowski and Moncrieff 2001) is shown in Fig.6f, which is characterized by anomalies in a front-to-rear tilt. In detail, the temperature anomalies have an elbow shape with upward/westward tilted structure below the level $z = 14km$ and upward/eastward tilted structure above that level, which is reminiscent of the typical temperature anomalies associated with CCEWs as observed in nature (Kiladis et al. 2009). The maximum temperature perturbations are about 0.8 $K$ and the minimum temperature perturbations are about -0.6 $K$, both of which are located in the upper troposphere. Such potential temperature anomalies can be either driven by mean heating or eddy transfer of momentum and temperature, or both of them. To figure out this question, potential temperature anomalies induced by mean heating, EMT and EHT are discussed separately and the total anomalies are compared directly with those from the study (Grabowski and Moncrieff 2001).

Physically, latent heat release during tropical precipitation starts from the low-level congestus clouds to deep convective clouds to upper-level stratiform clouds (Khouider and Majda 2008b). Thus mean heating is prescribed as follows,

$$\left\langle \bar{S}^{\theta} \right\rangle = c_0 \left[ \sin\left(\frac{10\pi\left(X-st\right)}{L}\right)\sin\left(z\right) - \frac{2}{3}\sin\left(\frac{10\pi\left(X-st\right)}{L}+\frac{\pi}{2}\right)\sin\left(2z\right)\right], \tag{21}$$

where magnitude coefficient $c_0 = 0.5$ corresponds to 5 $Kday^{-1}$. $s = \frac{4}{25}$ (8 $ms^{-1}$) is the propagation speed of the envelope. Eq.21 also assumes that the convective envelope $E\left(X-st\right)$ in Eq.18 is in phase with the first baroclinic mode (deep convection) of mean heating.

Fig.5 shows the prescribed mean heating and the resulting zonal/vertical velocity in the longitude-height diagram at 41.5 $day$. The alternate heating and cooling regions are upward/westward tilted. Upward/westward motion dominates in heating regions, while downward/eastward motion dominates in cooling regions. Such upward/westward tilted vertical structure of zonal velocity is quite often observed in the reality (Kiladis et al. 2009). As for the vertical velocity, the upward (downward) motion is in phase with the heating (cooling) regions, which is reminiscent of the realistic process in nature when air parcels gain buoyancy and lift up during latent heat release. Besides, wind convergence (divergence) occurs in the leading edge of heating (cooling) regions and trailing edge of cooling (heating) regions. In a moist environment, such wind convergence in the leading edge tends to trap moisture and bring them along with the inflow to the upper levels.

Fig.6a shows potential temperature anomalies induced by mean heating in the longitude-height diagram at 41.5 $day$. Again, the spatial pattern of potential temperature anomalies is characterized by the upward/westward tilted vertical structure. Besides, opposite potential temperature anomalies are induced in the upper and lower tropospheres, indicating the significant synoptic-scale circulation response in the second baroclinic mode. Also, the maximum magnitude of potential temperature anomalies is reached in the lower troposphere at the height 4 *km* and upper troposphere at the height 12 *km*. Such potential temperature anomalies are quite different from those in the study (Grabowski and Moncrieff 2001).

Fig.6b potential temperature anomalies induced by EMT in the longitude-height diagram at 41.5 *day*. The vertical profile of potential temperature anomalies is characterized by positive (negative) anomalies in the middle troposphere and negative (positive) anomalies in the upper and lower tropospheres, indicating the significant strength of the third baroclinic mode. Fig.6d shows potential temperature anomalies induced by EHT in the longitude-height diagram at 41.5 *day*. The maximum magnitude of potential temperature anomalies induced by EHT is much weaker than that by EMT, which can be explained by the slow phase speed of mesoscale heating in Eq.16. Besides, potential temperature anomalies induced by EMT and EHT are almost opposite to each other, resulting in weaker magnitude of total potential temperature anomalies.

Fig.6c shows relative location between potential temperature anomalies induced by eddy terms and those induced by mean heating in the longitude-height diagram at 41.5 *day*. In the lower troposphere, the anomalies induced by eddy terms and mean heating overlap each other but in the opposite signs, resulting in diminishing potential temperature anomalies below the height 5 *km*. In fact, such diminishing potential temperature anomalies is apparent in Fig.6f from the study (Grabowski and Moncrieff 2001). In the middle troposphere, potential temperature anomalies induced by eddy terms tends to strengthen anomalies induced by mean heating. In the upper troposphere, potential temperature anomalies induced by eddy terms are out of phase with those anomalies induced by mean heating, introducing the vertical shear of total potential temperature anomalies and contributing the upward/westward tilted structure. As shown by Fig.6e, the total potential temperatures anomalies are quite similar to those in Fig.6f from the study (Grabowski and Moncrieff 2001).

*c. Zonal velocity on the synoptic scale*

Fig.7f shows the spatial distribution of zonal velocity in the study (Grabowski and Moncrieff 2001). In the lower (upper) troposphere, there are weak easterly (westerly) wind anomalies in an upward/westward tilt. Besides, easterly wind anomalies exist between the strong westerly wind anomalies near the top of troposphere. Without changing any model setup and physical parameters, the goal of this section is to explore whether the total zonal velocity induced by mean heating and eddy terms owns some similar features as Fig.7f.

Fig.7a shows zonal velocity induced by mean heating in the longitude-height diagram at 41.5 *day*. In connection with Fig.5, heating regions are mostly dominated by easterly wind anomalies, while cooling regions are mostly dominated by westerly wind anomalies. At the surface, there are easterly (westerly) wind anomalies to the east (west) of the heating regions, resulting in wind convergence. Such upward/westward tilted zonal velocity features the significant magnitude of the first and second baroclinic modes. When compared with Fig.7f, there exist many discrepancies of zonal velocity anomalies such as the strong westerlies in the lower troposphere.

Fig.7b shows the zonal velocity induced by EMT in the longitude-height diagram at 41.5 *day*, which is characterized by low-level easterly winds and upper-level westerly winds. Near the vertical boundaries, westerly (easterly) wind anomalies in weak magnitude are also induced at the surface (top). Fig.7d shows zonal velocity induced by EHT in the longitude-height diagram at 41.5 *day*. The maximum magnitude of zonal velocity is much weaker than that in Fig.7b. The total zonal velocity induced by EMT and EHT is shown in Fig.7c, whose the maximum upper-level westerlies and low-level easterlies are displaced to the west, due to zonal velocity anomalies induced by EHT in the opposite sign.

Fig.7c shows relative location between the zonal velocity induced by mean heating and that induced by eddy terms in the longitude-height diagram at 41.5 *day*. In the upper troposphere between the height 8 *km* and 13 *km*, westerly wind anomalies induced by eddy terms dominates, which tends to strengthen westerlies and weaken easterlies induced by mean heating. The resulting total westerly wind anomalies in Fig.7e have upward/westward tilted vertical structure in the upper troposphere. Similarly, easterly wind anomalies induced by eddy terms dominate in the lower troposphere and the resulting total easterly wind anomalies have upward/westward tilted vertical structure. Near the upper boundary, there also exist alternate easterly and westerly wind anomalies. All these features in the upper and lower tropospheres resemble those in Fig.7f, except for the extra westerly wind anomalies at the surface. One possible reason for such discrepancy is the missing boundary layer dynamics in the MESD model but well resolved in the cloud resolving model (Grabowski and Moncrieff 2001).

### *d. Vertical velocity on the synoptic scale*

Fig.8d shows the spatial distribution of vertical velocity in the study (Grabowski and Moncrieff 2001). The most significant vertical motion is located in the middle and upper tropospheres with the maximum value at height 12 *km*. In contrast to potential temperature anomalies and zonal velocity in an upward/westward tilt, the vertical profile of vertical motion is mostly upright. Without changing any model setup and physical parameters, the goal of this section is to explore whether the total vertical velocity induced by mean heating and eddy terms has some similar features as Fig.8f.

Fig.8a-b show vertical velocity induced by EMT and EHT in the longitude-height diagram at 41.5 *day*. Particularly, vertical velocity induced by eddy terms has very weak magnitude and cancels each other in the opposite sign. In contrast, vertical velocity induced by mean heating dominates in a comparable magnitude as Fig.8d. However, such front-to-rear tilted vertical motion is quite different from the upright vertical motion in the study (Grabowski and Moncrieff 2001). The next section is used to investigate whether upright mean heating will induce such upright vertical motion and whether the upward/westward tilted vertical structure of potential temperature anomalies and zonal velocity in the previous discussion is still captured in the existence of upright mean heating and eddy terms.

## 5. Upright Mean Heating

According to the observation (Straub and Kiladis 2002; Kiladis et al. 2009), the dynamical fields such as the zonal wind, temperature and specific humidity of convectively coupled Kelvin waves have the upward/westward tilted vertical structure as they propagate eastward. Three cloud types with low-level congestus clouds in the leading edge, deep convective clouds in the middle and upper-level stratiform clouds in the trailing edge provides the key components for the tilted vertical structure. However, Fig.8 suggests that the upright mean heating can induce upright vertical motion on the large-scale domain. In this section, an elevated upright mean heating is used to investigate whether both upright vertical velocity and upward/westward tilted zonal velocity and potential temperature anomalies can still be captured in the existence of upright mean heating and eddy terms.

In the tropics, deep convective clouds can warm and dry the entire troposphere through large amounts of rainfall. Besides, the stratiform clouds warm and dry the upper troposphere through stratiform precipitation and cool and moisten the lower troposphere due to the rain evaporation

(Khouider and Majda 2008b). Thus the latent heat release associated with in-phase deep and stratiform convection is characterized by an elevated upright mean heating. In fact, it has been confirmed by model experiments that diabatic processes in deep convective and stratiform regions are essential to the formation of multiscale convective wave patterns (Tulich and Mapes 2008). Here the vertical profile of the elevated upright mean heating is prescribed as follows,

$$G(z) = c_0 \left[\sin(z) - 0.6\sin(2z)\right] \tag{22}$$

where the heating magnitude $c_0 = 0.5$ corresponds to 5 $Kday^{-1}$.

Fig.9 shows the elevated upright mean heating in the longitude-height diagram at 41.5 *day*. The maximum magnitude of heating and cooling is achieved in the upper troposphere around 6 $Kday^{-1}$. Fig.9b shows vertical velocity induced by such an elevated upright mean heating in the longitude-height diagram at 41.5 *day*. Similar to the mean heating, the vertical motion reaches its maximum value in the upper troposphere at the height 12 *km* and decays as the height goes close to the top and lower troposphere. More importantly, it is quite similar to Fig.8d in the study (Grabowski and Moncrieff 2001), providing a convincing evidence for the upright mean heating on the synoptic scale.

Fig.9c shows potential temperature anomalies induced by upright mean heating and eddy terms in the longitude-height diagram at 41.5 *day*. Similar to those induced by upward/westward tilted mean heating in Fig.6a, potential temperature anomalies induced by upright mean heating are also characterized by opposite anomalies between the upper and lower tropospheres, indicating the significant magnitude of the second baroclinic mode. Instead of an upward/west tilt, their vertical profile has an upward/eastward tilt. After combined with those induced by eddy terms, the total potential temperature anomalies as shown in Fig.9d exhibit an upward/westward tilt again with the maximum value in the height 10 $km$. Such potential temperature anomalies are quite similar to those in Fig.6f, except that the magnitude of upper-level anomalies here is much weaker.

Fig.9e shows zonal velocity induced by upright mean heating and eddy terms in the longitude-height diagram at 41.5 $day$. In the heating region near the longitude $10^4 km$, there are wind convergence in the middle troposphere at the height 7.85 $km$ and wind divergence at the top of troposphere. The wind strength at lower levels is negligible, due to the elevated height of mean heating. After combined with that induced by eddy terms, the total zonal velocity as shown in Fig.9f is characterized by upper-level westerlies on top of low-level easterlies. At the top of the troposphere, there exist alternate easterlies and westerlies in strong magnitudes. The overall spatial pattern of zonal velocity is quite similar to that in Fig.7f, except for the upper-level westerlies in both upward/eastward and upward/westward tilts.

## 6. Eastward-Moving Convective Envelope in Faster Propagation Speeds

In the classic shallow water theory, the eastward-moving Kelvin waves in the first baroclinic mode has phase speed 50 $ms^{-1}$ (Matsuno 1966; Majda 2003). Because of moist processes, CCEWs such as convectively coupled Kelvin waves typically have shallower equivalent depth (slower phase speed). In general, the eastward-propagating convectively coupled Kelvin waves are observed to have phase speed $15-20 ms^{-1}$ over the west Pacific and $12-15 ms^{-1}$ over the Indian Ocean (Kiladis et al. 2009). Such slow propagation speeds of CCEWs become a benchmark to examine the behavior and skill of complex numerical simulations. In the two-dimensional cloud resolving simulations with a strong background easterlies winds (-10 $ms^{-1}$) (Grabowski and Moncrieff 2001), the large-scale envelope over a few thousand kilometers propagates west to east at about 6 to 8 $ms^{-1}$ relative to the earth, which is much slower than the phase speed of the convectively coupled Kelvin waves in nature. It is important to investigate discrepancies of flow fields between the slow and fast propagation speed scenarios. Specifically, a fast propagation scenario (18 $ms^{-1}$ for mean heating and mesoscale heating envelope) is considered here. All the other model setup is the same as Sec.4.

Fig.10a-d shows potential temperature anomalies induced by mean heating and eddy terms. Similar to Fig.6a, potential temperature anomalies induced by mean heating in Fig.10a also have an upward/westward tilted vertical profile in the fast scenario. The maximum magnitude of potential temperature anomalies in the fast propagation case ($1.2K$) is much stronger than that in the slow propagation speed ($0.8K$). In contrast to that, potential temperature anomalies induced by eddy terms in both cases have similar maximum magnitudes. The total potential temperature anomalies in Fig.10c has an clear upward/westward tilt. A further investigation for potential temperature anomalies in different propagation speed scenarios are shown in Fig.10d. It can be concluded that mean heating tends to induce stronger potential temperature anomalies in faster propagation speeds (less than 25 $ms^{-1}$), while anomalies induced by eddy terms do not change much. The propagation speed 25 $ms^{-1}$ as a threshold corresponds to the phase speed of gravity waves in the second baroclinic modes as discussed in Sec.2.

Fig.10e-h shows zonal velocity induced by upward/westward mean heating and eddy terms. Similar to Fig.7a in the slow scenario, zonal velocity induced by mean heating in Fig.10e also has an upward/westward tilted vertical profile in the fast scenario. However, the maximum magnitude of both the easterlies and westerlies in the fast scenario is 3.5 $ms^{-1}$, much stronger than than that in the slow propagation speed (2.5 $ms^{-1}$). The overall spatial pattern of zonal velocity induced by eddy terms in Fig.10f and the total zonal velocity in Fig.10g are quite similar to that in Fig.7c and Fig.7e. A further investigation for zonal velocity in different propagation speed scenarios are shown in Fig.10h. Similarly, it can be concluded that mean heating tends to induce stronger zonal velocity in the faster propagation speed (less than 25 $ms^{-1}$), while that induced by eddy terms does not change much.

## 7. Westward-Moving Mesoscale Heating in An Upward/Westward Tilt

One crucial feature of self-similarity of tropical convection is the front-to-rear tilted vertical structure, which is commonly observed in MCSs (Houze 2004) and CCEWs (Kiladis et al. 2009). In the two-dimensional cloud resolving simulations (Grabowski and Moncrieff 2001), the westward-moving systems are characterized by low-level inflow and upper-level outflow in an upward/eastward tilt. It is important to know why mesoscale systems with an upward/westward tilt are unfavorable and what is the underlying physical mechanism to avoid them. In order to prescribe such a westward-moving mesoscale system in an upward/westward tilt, here the expression of mesoscale heating is the same as Eq.19 except that the sign of phase shift is reversed $\phi_0 = \frac{\pi}{4}$. According to Eqs.12 and Eq.14, after switching the sign of phase shift parameter $\phi_0$ from $-\frac{\pi}{4}$ to $\frac{\pi}{4}$, both vertical profiles and magnitudes of EMT and EHT remains the same except for their signs. In other words, the synoptic-scale circulation response to eddy terms including potential temperature anomalies in Fig.6c and zonal velocity in Fig.7c has the same spatial pattern but the opposite sign.

Fig.11a shows relative location between mean heating and potential temperature anomalies induced by eddy terms in the longitude-height diagram at 41.5 *day*. In the lower troposphere, positive potential temperature anomalies induced by eddy terms are located to the east of mean heating as it propagates eastward. In a moist environment, such positive potential temperature anomalies can suppress convection through decreasing convective available potential energy (CAPE), increasing saturation rate of water vapor and convective inhibition (CIN). In the reality, the leading edge of the synoptic-scale convective envelope mostly consists of shallow congestus clouds in the lower troposphere. Therefore, the upscale impact of mesoscale fluctuations of momentum and temperature tends to suppress shallow convection in the leading edge and further destroy the multi-scale coherent structure of synoptic-scale equatorial waves. In the middle troposphere, potential temperature anomalies induced by eddy terms are out of phase with the mean heating. There are negative (positive) anomalies to the east (west), which favor (suppress) convection to the east (west). In the upper troposphere, the negative potential temperature anomalies in the upper-level mean heating region provide favorable conditions for stratiform convection.

Fig.11b shows relative location of potential temperature anomalies induced by mean heating and eddy terms in the longitude-height diagram at 41.5 $day$. In the lower troposphere in Fig.11c, potential temperature anomalies induced by eddy terms tend to strengthen those induced by mean heating, resulting in strong low-level anomalies with their maximum around $0.67K$. In the middle troposphere, potential temperature anomalies induced by eddy terms have dominate magnitudes and reverse the sign of those induced by mean heating. In connection to those in the upper troposphere, eddy terms induce upward/eastward tilted potential temperature anomalies in the upper levels. Fig.11 shows the total potential temperature anomalies induced by both mean heating and eddy terms. Such spatial pattern of potential temperature anomalies are quite different from Fig.6f from the study (Grabowski and Moncrieff 2001).

## 8. Concluding Discussion

Synoptic-scale equatorial waves coupled with tropical convection are typically organized in a hierarchy of multiple spatial and temporal scales (Kiladis et al. 2009). In particular, convectively coupled Kelvin waves are characterized by a eastward-moving convective envelope with embedded westward-moving mesoscale disturbances (Straub and Kiladis 2002). Such multi-scale coherent structure of tropical convection is simulated in the two-dimensional cloud resolving simulations (Grabowski and Moncrieff 2001). The first goal of this paper is using the two-dimensional

MESD model to capture the organized structure of large-scale circulation with westward-moving mesoscale systems embedded in an eastward-moving synoptic-scale convective envelope as simulated in (Grabowski and Moncrieff 2001). The second goal is to assess the upscale impact of mesoscale disturbances on the behavior of synoptic-scale circulation through eddy transfer of momentum and temperature. The third goal aims at understanding how much of synoptic-scale circulation is induced by eddy transfer of momentum and temperature rather than synoptic-scale mean heating.

The two-dimensional MESD model is reduced from the three-dimensional MESD model (Majda 2007) by following several simplifying assumptions. After ignoring all the forcing terms, both mesoscale and synoptic-scale governing equations share the same gravity wave equations as their dynamic core, indicating the self-similarity of flow fields and tropical convection as emphasized in (Majda 2007). In particular, the synoptic-scale equations are forced by mean heating and eddy transfer of momentum and temperature, where the latter represents upscale impact of mesoscale disturbances on the synoptic-scale circulation. After implementing similar model setup as (Grabowski and Moncrieff 2001), the synoptic-scale circulation response from the two-dimensional MESD model is directly compared with results from (Grabowski and Moncrieff 2001). Besides, three different scenarios with elevated upright mean heating, a faster propagating convective envelope and westward-moving mesoscale heating in an upward/westward tilt are considered and used to achieve those goals as mentioned before.

On the mesoscale, as driven by a prescribed westward-moving top-heavy mesoscale heating in an upward/eastward tilt, the mesoscale flow fields share many similar features with the westward-moving mesoscale systems in (Grabowski and Moncrieff 2001), including the tilted low-level inflow and upper-level outflow. The associated EMT is characterized by upper-level (low-level) eastward (westward) momentum forcing, while EHT is manifested by mid-level cooling and upper-level/low-level heating. The relative strength of synoptic-scale circulation response induced by EMT and EHT is determined by the propagation speed of mesoscale heating in the MESD model.

On the synoptic scale, mesoscale heating is modulated by a zonally varying large-scale envelope, which propagates eastward in the same speed as the mean heating. Many features of flow fields simulated by Grabowski and Moncrieff (2001) are captured here. First, the domain-averaged zonal velocity at each level is characterized by upper-level westerlies and low-level easterlies, which is just generated by EMT. Secondly, EMT and EHT tend to induce synoptic-scale circulation in the opposite signs, although that induced by EMT dominates in the slow mesoscale heating scenario. The total potential temperature anomalies induced by mean heating and eddy terms have an upward/westward tilt. Also, the total zonal velocity is characterized by westerlies on top of easterlies in tilted vertical structure. Thirdly, compared with eddy terms, synoptic-scale mean heating induces tilted vertical motion in much stronger magnitude, which is quite different from the upright vertical motion as simulated in (Grabowski and Moncrieff 2001).

In the scenario with elevated upright mean heating, the synoptic-scale circulation response to mean heating and eddy terms includes potential temperature anomalies and zonal velocity in an upward/westward tilt and upright vertical velocity, similar to that in (Grabowski and Moncrieff 2001). Such a scenario highlights the significant upscale impact of mesoscale disturbances on the synoptic-scale circulation and supports the hypothesis that the front-to-rear tilted vertical structure of large-scale flow field can be contributed by eddy terms, even in the existence of upright mean heating.

In the scenario with a faster propagating convective envelope (less than 25 $ms^{-1}$) in Fig.10, the synoptic-scale circulation response to mean heating becomes stronger, while that driven by eddy terms does not change much. In other words, the upscale impact of mesoscale disturbances becomes less important as the propagation speed of convective envelope increases. Such a discussion can explain discrepancies of numerical results in cloud resolving models. For example, a strong easterly mean flow (-10 $ms^{-1}$) for the trade wind regime is assumed in the simulations by Grabowski and Moncrieff (2001), where CMT significantly modify the momentum budget of the large-scale flow and induces vertical shear of zonal momentum. The large-scale organization of convection propagates eastward slowly (8 $ms^{-1}$), in agreement with the conclusion that upscale impact of mesoscale disturbances plays an important role in the slow propagation scenario. In contrast, zero mean flow for the state of rest regime is assumed in the simulations by Tulich and Mapes (2008), where the upscale transport of horizontal momentum by coherent eddy circulations is found to be small. The horizontally propagating wave packets with roughly a full-wavelength structure in the troposphere has phase speed in the range 16-18 $ms^{-1}$, in agreement with the conclusion from the MESD model that the synoptic-scale circulation response to the mean heating dominates in the fast propagation scenario.

In the scenario with upward/westward tilted mesoscale heating, positive potential temperature anomalies are induced in the leading edge of the synoptic-scale mean heating by the upscale impact of mesoscale disturbances, which tends to suppress shallow convection through increasing saturation rate of vapor and CIN in a moist environment. Since shallow convection in the leading edge of large-scale convective envelope serves to moisten and precondition deep convection, such unfavorable conditions will destroy the multi-scale coherent structure of synoptic-scale equatorial waves, explaining the fact that westward-moving mesoscale heating in an upward/westward tilt is rarely observed in reality.

This study based on a simple multi-scale model has several implication for physical interpretation and comprehensive numerical models. In particular, the explicit expressions for EMT and EHT provide assessment of upscale impact of mesoscale disturbances on the synoptic-scale circulation in a transparent fashion, which should be useful to improve convective parameterization of organized tropical convection in the GCMs. The two-dimensional MESD model under the current model setup can also be generalized in several ways. One promising research direction is to consider the original three-dimensional MESD model with Coriolis force on the synoptic scale. In the existence of Kelvin waves, Rossby waves, MRG waves and Gravity waves, more realistic features are expected to be reproduced in this three-dimensional MESD model such as the zonal asymmetry of flow fields between eastward and westward propagating scenarios. Besides, by considering an off-equator convective envelope, it is also possible to mimic the scenario when CCEWs goes along the climatological ITCZ over the central and eastern Pacific.

*Acknowledgments.* This research of A.J.M is partially supported by the office of NAVAL Research ONR MURI N00014-12-1-0912, and Q.Y. is supported as a graduate research assistant on this grant.

APPENDIX

**Gravity waves on the mesoscale and their upscale fluxes**

It is proved here that free gravity waves in Eqs.1a-1d cannot generate nonzero EMT and EHT. In order to solve this system analytically, an ansatz for plane waves in the baroclinic mode is assumed as follows,

$$f = \tilde{f} e^{i(kx-\omega\tau)} \cos(qz), f \in \{u, v, p\} \tag{A1}$$

$$g = \tilde{g} e^{i(kx-\omega\tau)} \left[-q\sin(qz)\right], g \in \{w, \theta\} \tag{A2}$$

where $k$ is the wavenumber and $\omega$ is frequency. $q = 1, 2, 3...$ is the vertical index.

As shown in Eq.12 and Eq.14, both EMT and EHT are in the quadratic form between vertical velocity $w$ and zonal velocity $u$ (or potential temperature anomalies $\theta$). According to the definition of mesoscale zonal and temporal averaging in Eqs.3-4, two necessary conditions for nonzero eddy terms are,

$$|k_1| = |k_2| \tag{A3}$$

$$|\omega_1| = |\omega_2| \tag{A4}$$

where $k_1, \omega_1$ are for vertical velocity $w$ and $k_2, \omega_2$ are for $u$ (or $\theta$). According to the dispersion relation in Eq.9, the necessary conditions in Eqs.A3-A4 further imply,

$$|q_1| = |q_2| \tag{A5}$$

which requires that $w$ and $u$ (or $\theta$) are in the same baroclinic mode.

After plugging the ansatz in Eqs.A1-A2, the mesoscale equations in Eqs.1a-1d can be reduced to,

$$-i\omega\tilde{u} + ik\tilde{p} = 0 \tag{A6a}$$

$$-i\omega\tilde{\theta} + \tilde{w} = 0 \tag{A6b}$$

$$\tilde{p} = \tilde{\theta} \tag{A6c}$$

$$ik\tilde{u} - q^2\tilde{w} = 0 \tag{A6d}$$

According to Eq.A6b and Eq.A6d, it can be concluded that $w$ and $u$ ($w$ and $\theta$) are out of phase by $\frac{\pi}{2}$. Such an out-of-phase relation means that the value of EMT and EHT after taking mesoscale averaging should vanish.

## References


Biello, J. A., and A. J. Majda, 2010: Intraseasonal multi-scale moist dynamics of the tropical atmosphere. *Communications in Mathematical Sciences*, **8 (2)**, 519–540.

Chen, S. S., R. A. Houze Jr, and B. E. Mapes, 1996: Multiscale variability of deep convection in realation to large-scale circulation in toga coare. *Journal of the Atmospheric Sciences*, **53 (10)**, 1380–1409.

Deser, C., 1993: Diagnosis of the surface momentum balance over the tropical pacific ocean. *Journal of climate*, **6 (1)**, 64–74.

Grabowski, W. W., and M. W. Moncrieff, 2001: Large-scale organization of tropical convection in two-dimensional explicit numerical simulations. *Quarterly Journal of the Royal Meteorological Society*, **127 (572)**, 445–468.

Grabowski, W. W., X. Wu, and M. W. Moncrieff, 1996: Cloud-resolving modeling of tropical cloud systems during phase iii of gate. part i: Two-dimensional experiments. *Journal of the atmospheric sciences*, **53 (24)**, 3684–3709.

Houze, R. A., 2004: Mesoscale convective systems. *Reviews of Geophysics*, **42 (4)**.

Houze Jr, R. A., 1975: Squall lines observed in the vicinity of the researcher during phase iii of gate. *Preprints, 16th Radar Meteorology Conf., Houston, TX, American Meteorological Society*, 206–209.

Houze Jr, R. A., 1977: Structure and dynamics of a tropical squall-line system. *Monthly Weather Review*, **105 (12)**, 1540–1567.

Houze Jr, R. A., and C.-P. Cheng, 1977: Radar characteristics of tropical convection observed during gate: Mean properties and trends over the summer season. *Monthly Weather Review*, **105 (8)**, 964–980.

Jiang, X., and Coauthors, 2015: Vertical structure and physical processes of the madden-julian oscillation: Exploring key model physics in climate simulations. *Journal of Geophysical Research: Atmospheres*, **120 (10)**, 4718–4748.

Johnson, R. H., T. M. Rickenbach, S. A. Rutledge, P. E. Ciesielski, and W. H. Schubert, 1999: Trimodal characteristics of tropical convection. *Journal of climate*, **12 (8)**, 2397–2418.

Khouider, B., and Y. Han, 2013: Simulation of convectively coupled waves using wrf: a framework for assessing the effects of mesoscales on synoptic scales. *Theoretical and Computational Fluid Dynamics*, **27 (3-4)**, 473–489.

Khouider, B., Y. Han, and J. A. Biello, 2012: Convective momentum transport in a simple multicloud model for organized convection. *Journal of the Atmospheric Sciences*, **69 (1)**, 281–302.

Khouider, B., and A. J. Majda, 2006a: Model multi-cloud parameterizations for convectively coupled waves: Detailed nonlinear wave evolution. *Dynamics of atmospheres and oceans*, **42 (1)**, 59–80.

Khouider, B., and A. J. Majda, 2006b: A simple multicloud parameterization for convectively coupled tropical waves. part i: Linear analysis. *Journal of the atmospheric sciences*, **63 (4)**, 1308–1323.

Khouider, B., and A. J. Majda, 2007: A simple multicloud parameterization for convectively coupled tropical waves. part ii: Nonlinear simulations. *Journal of the atmospheric sciences*, **64 (2)**, 381–400.

Khouider, B., and A. J. Majda, 2008a: Equatorial convectively coupled waves in a simple multicloud model. *Journal of the Atmospheric Sciences*, **65 (11)**, 3376–3397.

Khouider, B., and A. J. Majda, 2008b: Multicloud models for organized tropical convection: Enhanced congestus heating. *Journal of the Atmospheric Sciences*, **65 (3)**, 895–914.

Kiladis, G. N., M. C. Wheeler, P. T. Haertel, K. H. Straub, and P. E. Roundy, 2009: Convectively coupled equatorial waves. *Reviews of Geophysics*, **47 (2)**.

Majda, A., 2003: *Introduction to PDEs and Waves for the Atmosphere and Ocean*, Vol. 9. American Mathematical Soc.

Majda, A. J., 2007: New multiscale models and self-similarity in tropical convection. *Journal of the atmospheric sciences*, **64 (4)**, 1393–1404.

Majda, A. J., and R. Klein, 2003: Systematic multiscale models for the tropics. *Journal of the Atmospheric Sciences*, **60 (2)**, 393–408.

Majda, A. J., and S. N. Stechmann, 2008: Stochastic models for convective momentum transport. *Proceedings of the National Academy of Sciences*, **105 (46)**, 17 614–17 619.

Majda, A. J., and S. N. Stechmann, 2009: A simple dynamical model with features of convective momentum transport. *Journal of the Atmospheric Sciences*, **66 (2)**, 373–392.

Majda, A. J., and Q. Yang, 2016: A multiscale model for the intraseasonal impact of the diurnal cycle over the maritime continent on the madden–julian oscillation. *Journal of the Atmospheric Sciences*, **73 (2)**, 579–604.

Mapes, B., S. Tulich, J. Lin, and P. Zuidema, 2006: The mesoscale convection life cycle: Building block or prototype for large-scale tropical waves? *Dynamics of atmospheres and oceans*, **42 (1)**, 3–29.

Matsuno, T., 1966: Quasi-geostrophic motions in the equatorial area. *J. Meteor. Soc. Japan*, **44 (1)**, 25–43.

Moncrieff, M. W., D. E. Waliser, M. J. Miller, M. A. Shapiro, G. R. Asrar, and J. Caughey, 2012: Multiscale convective organization and the yotc virtual global field campaign. *Bulletin of the American Meteorological Society*, **93 (8)**, 1171–1187.

Nakazawa, T., 1988: Tropical super clusters within intraseasonal variations over the western pacific. *J. Meteor. Soc. Japan*, **66 (6)**, 823–839.

Romps, D. M., 2014: Rayleigh damping in the free troposphere. *Journal of the Atmospheric Sciences*, **71 (2)**, 553–565.

Straub, K. H., and G. N. Kiladis, 2002: Observations of a convectively coupled kelvin wave in the eastern pacific itcz. *Journal of the atmospheric sciences*, **59 (1)**, 30–53.

Straub, K. H., G. N. Kiladis, and P. E. Ciesielski, 2006: The role of equatorial waves in the onset of the south china sea summer monsoon and the demise of el niño during 1998. *Dynamics of atmospheres and oceans*, **42 (1)**, 216–238.

Tao, W.-K., and M. W. Moncrieff, 2009: Multiscale cloud system modeling. *Reviews of Geophysics*, **47 (4)**.

Tulich, S. N., and B. E. Mapes, 2008: Multiscale convective wave disturbances in the tropics: Insights from a two-dimensional cloud-resolving model. *Journal of the Atmospheric Sciences*, **65 (1)**, 140–155.

Tung, W.-W., and M. Yanai, 2002a: Convective momentum transport observed during the toga coare iop. part i: General features. *Journal of the atmospheric sciences*, **59 (11)**, 1857–1871.

Tung, W.-W., and M. Yanai, 2002b: Convective momentum transport observed during the toga coare iop. part ii: Case studies. *Journal of the atmospheric sciences*, **59 (17)**, 2535–2549.

Wang, H., and R. Fu, 2007: The influence of amazon rainfall on the atlantic itcz through convectively coupled kelvin waves. *Journal of climate*, **20 (7)**, 1188–1201.

Wheeler, M., G. N. Kiladis, and P. J. Webster, 2000: Large-scale dynamical fields associated with convectively coupled equatorial waves. *Journal of the Atmospheric Sciences*, **57 (5)**, 613–640.

Yang, Q., and A. J. Majda, 2014: A multi-scale model for the intraseasonal impact of the diurnal cycle of tropical convection. *Theoretical and Computational Fluid Dynamics*, **28 (6)**, 605–633.

Zhang, C., 2005: Madden-julian oscillation. *Reviews of Geophysics*, **43 (2)**.

## LIST OF TABLES

| | Physical variables | Symbolic notation | Value |
|---|---|---|---|
| Synoptic scale | Zonal scale | $X$ | 1500 $km$ |
| | Temporal scale | $t$ | 8.3 $h$ |
| | Zonal velocity | $U$ | 5 $ms^{-1}$ |
| | Vertical velocity | $W$ | $1.6 \times 10^{-2}$ $ms^{-1}$ |
| | Pressure perturbation | $P$ | 250 $m^2s^{-2}$ |
| | Potential temperature anomalies | $\Theta$ | 3.3 $K$ |
| | Zonal momentum forcing | $S^u$ | 15 $ms^{-1}day^{-1}$ |
| | Thermal forcing | $S^\theta$ | 10 $Kday^{-1}$ |
| Mesoscale | Zonal scale | $x$ | 150 $km$ |
| | Temporal scale | $\tau$ | 50 $min$ |
| | Zonal velocity | $u$ | 5 $ms^{-1}$ |
| | Vertical velocity | $w$ | $1.6 \times 10^{-1}$ $ms^{-1}$ |
| | Pressure perturbation | $p$ | 250 $m^2s^{-2}$ |
| | Potential temperature anomalies | $\theta$ | 3.3 $K$ |
| | Zonal momentum forcing | $s_u$ | 150 $ms^{-1}day^{-1}$ |
| | Thermal forcing | $s_\theta$ | 100 $Kday^{-1}$ |

TABLE 1. The parameters, constant and scaling of physical variables in the two-dimensional MESD model.

| Resolution | Notation | Value |
|---|---|---|
| Zonal length | $L$ | 20,000 *km* |
| Vertical length | $H$ | 15.7 *km* |
| Total time | $T$ | 41.5 *day* |
| x-grid number | $N_x$ | 201 |
| x-grid spacing | $\Delta x$ | 100 *km* |
| z-grid number | $Nz$ | 31 |
| z-grid spacing | $\Delta z$ | 0.5 *km* |
| Time step | $N_t$ | 3600 |
| Time interval | $\Delta t$ | 16.6 *min* |

TABLE 2. Grid number and time steps in solving the synoptic-scale equations in the two-dimensional MESD model.

# LIST OF FIGURES

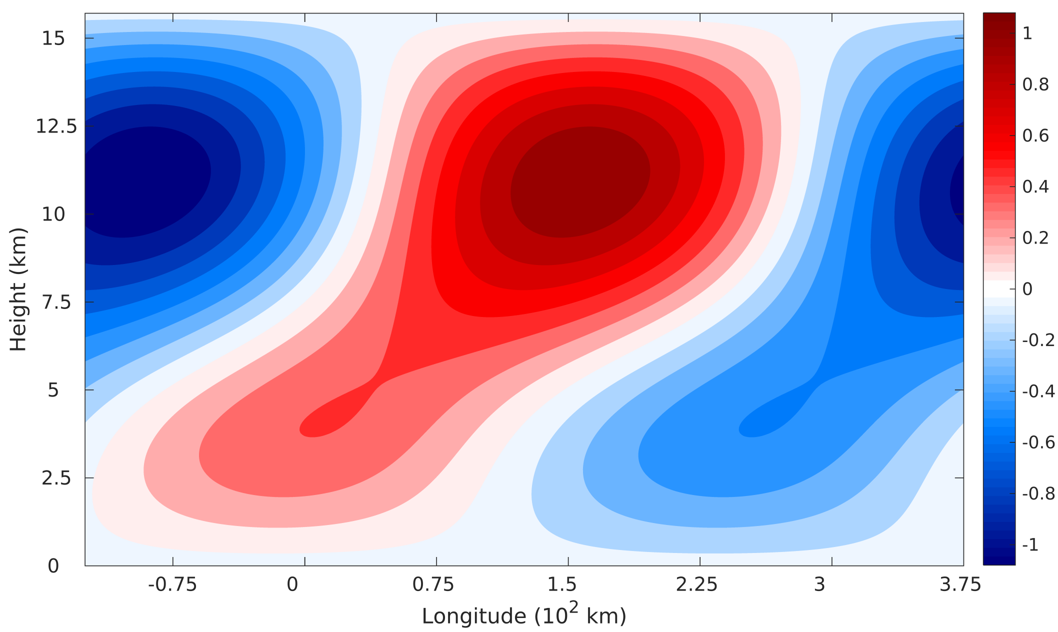


FIG. 1. Spatial pattern of westward-moving mesoscale heating in the longitude-height diagram. One dimensionless unit corresponds to $100 K day^{-1}$.

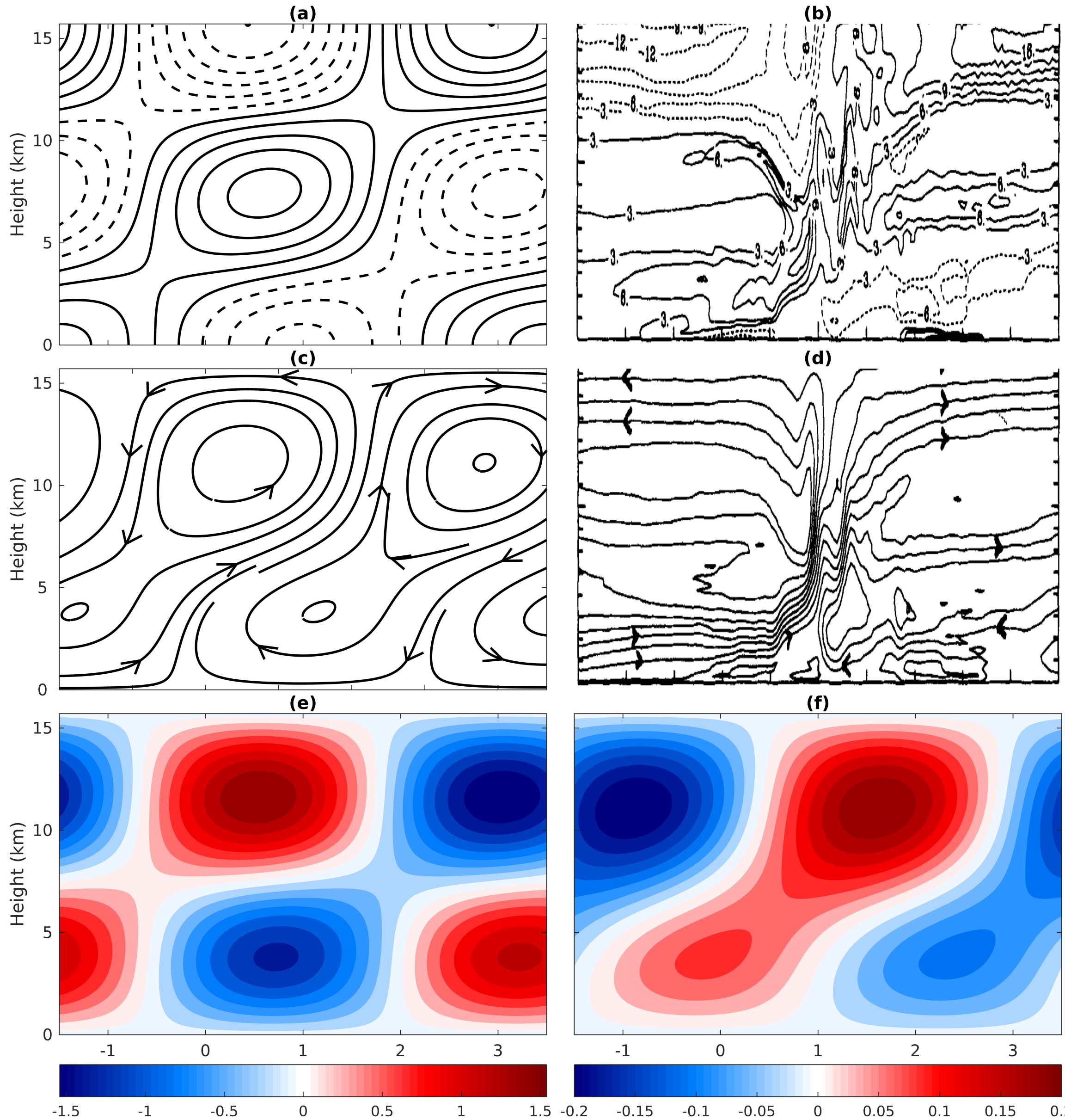


FIG. 2. Zonal velocity, vertical velocity and potential temperature anomalies on the mesoscale in the longitude-height diagram. The panels show (a-b) zonal velocity, (c-d) streamfunction, (e) potential temperature anomalies, (f) vertical velocity. Panels (b,d) show Figure 4b and Figure 4c from the paper (Grabowski and Moncrieff 2001). The contour interval of zonal velocity is 0.98 $ms^{-1}$. The dimensional units of zonal velocity, vertical velocity and potential temperature anomalies are $ms^{-1}$, $ms^{-1}$, $K$.

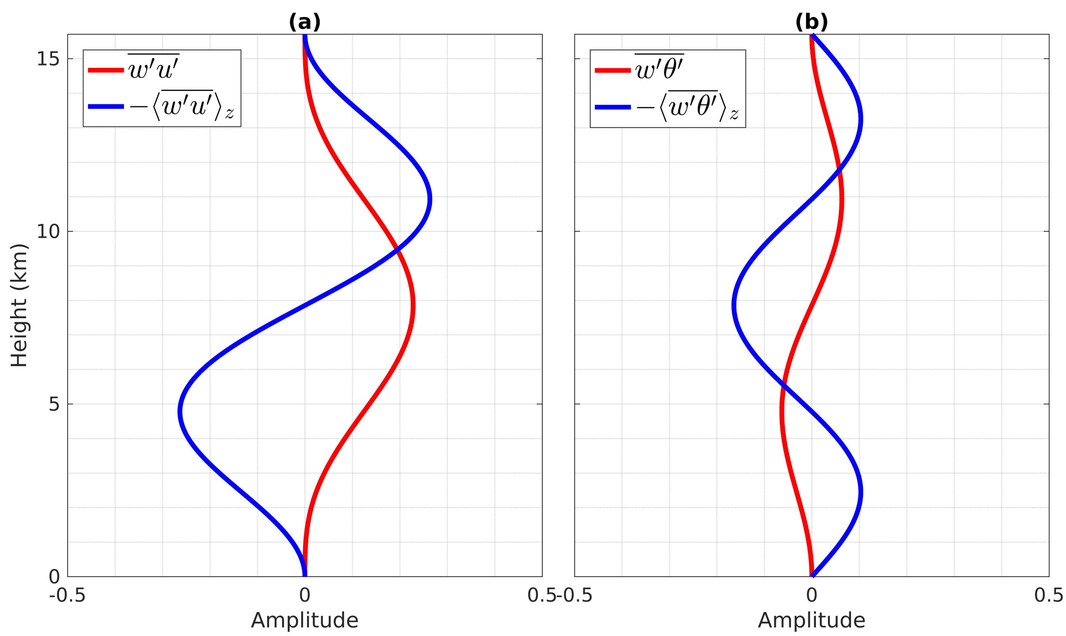


FIG. 3. Vertical structure of (a) eddy momentum transfer and (b) eddy heat transfer. In each panel, the red curve is for eddy fluxes and blue curve is for vertical gradient of eddy fluxes in a minus sign. One dimensionless unit of eddy momentum transfer is $15ms^{-1}day^{-1}$ and that of eddy heat transfer is $10Kday^{-1}$.

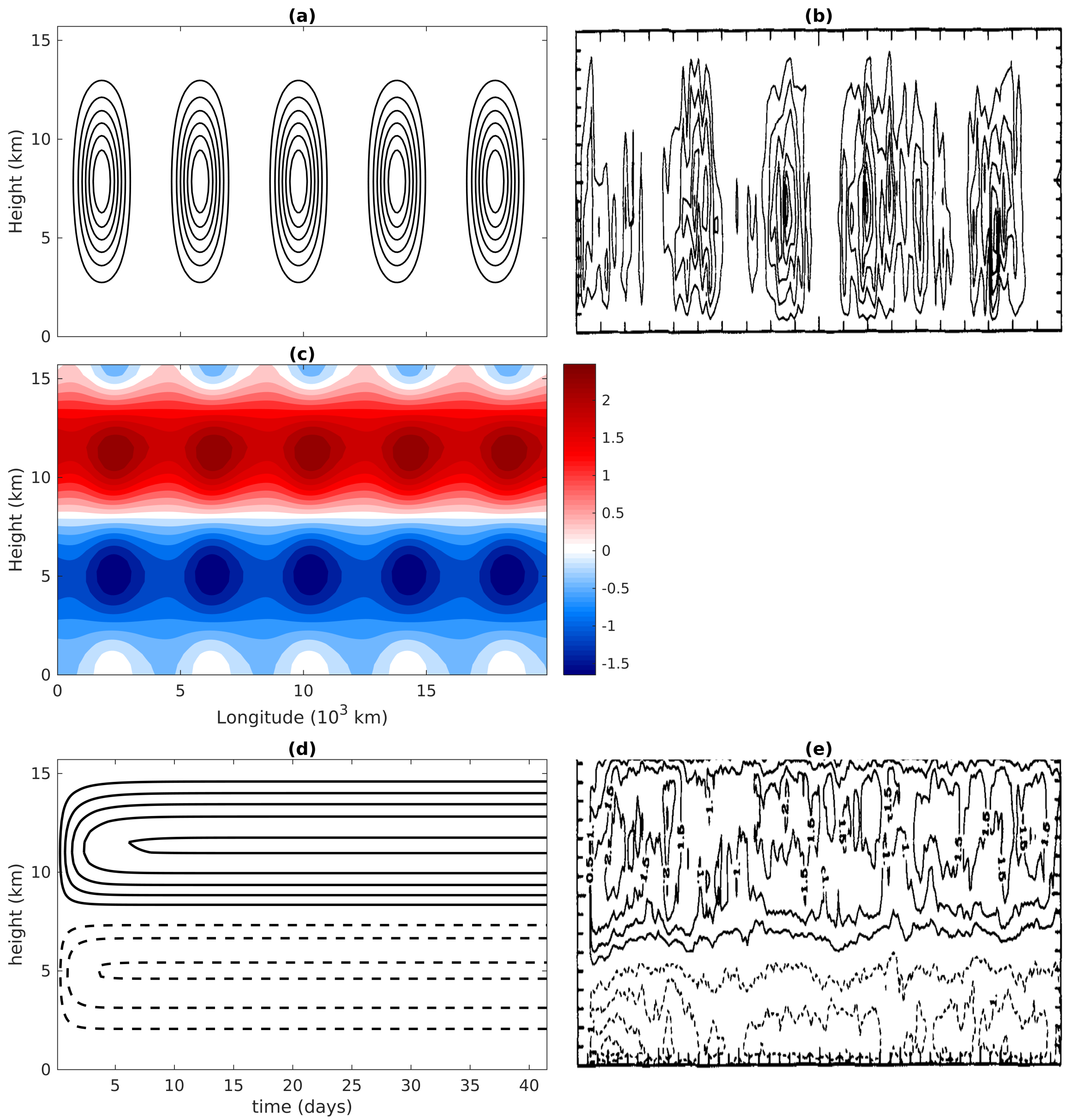


FIG. 4. Spatial distribution of momentum flux and zonal velocity at 41.5 *day* and time series of domain-averaged zonal momentum. The left column shows numerical solutions and the right column shows Figure 16a and Figure 17a from the paper (Grabowski and Moncrieff 2001). The panels show (a-b) momentum flux, (c) zonal velocity, (d-e) domain-averaged zonal momentum. The contour interval in panels is (a) 0.03 $m^2s^{-2}$, (b) 0.02 $Nm^{-2}$,(d) 0.42 $ms^{-1}$, (e) 0.5 $ms^{-1}$. The dimensional units of momentum flux, zonal velocity in the numerical solutions are $m^2s^{-2}$ and $ms^{-1}$.

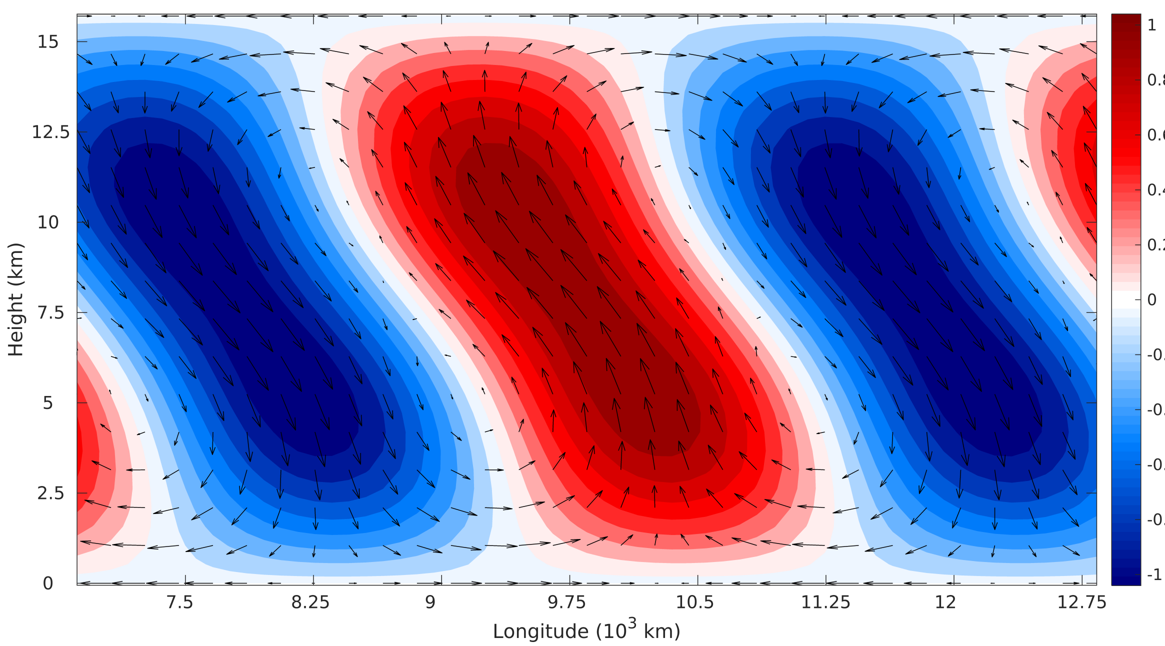


FIG. 5. Mean heating (color) and zonal/vertical velocity (arrow) in the longitude-height diagram at 41.5 *day*. Only the solutions in the longitude range from $6.87 \times 10^3 km$ to $12.84 \times 10^3 km$ are plotted here. The maximum magnitude of zonal and vertical velocity are $1.92 ms^{-1}$ and $0.89 cms^{-1}$. The dimensional unit of mean heating is $10\ Kday^{-1}$.

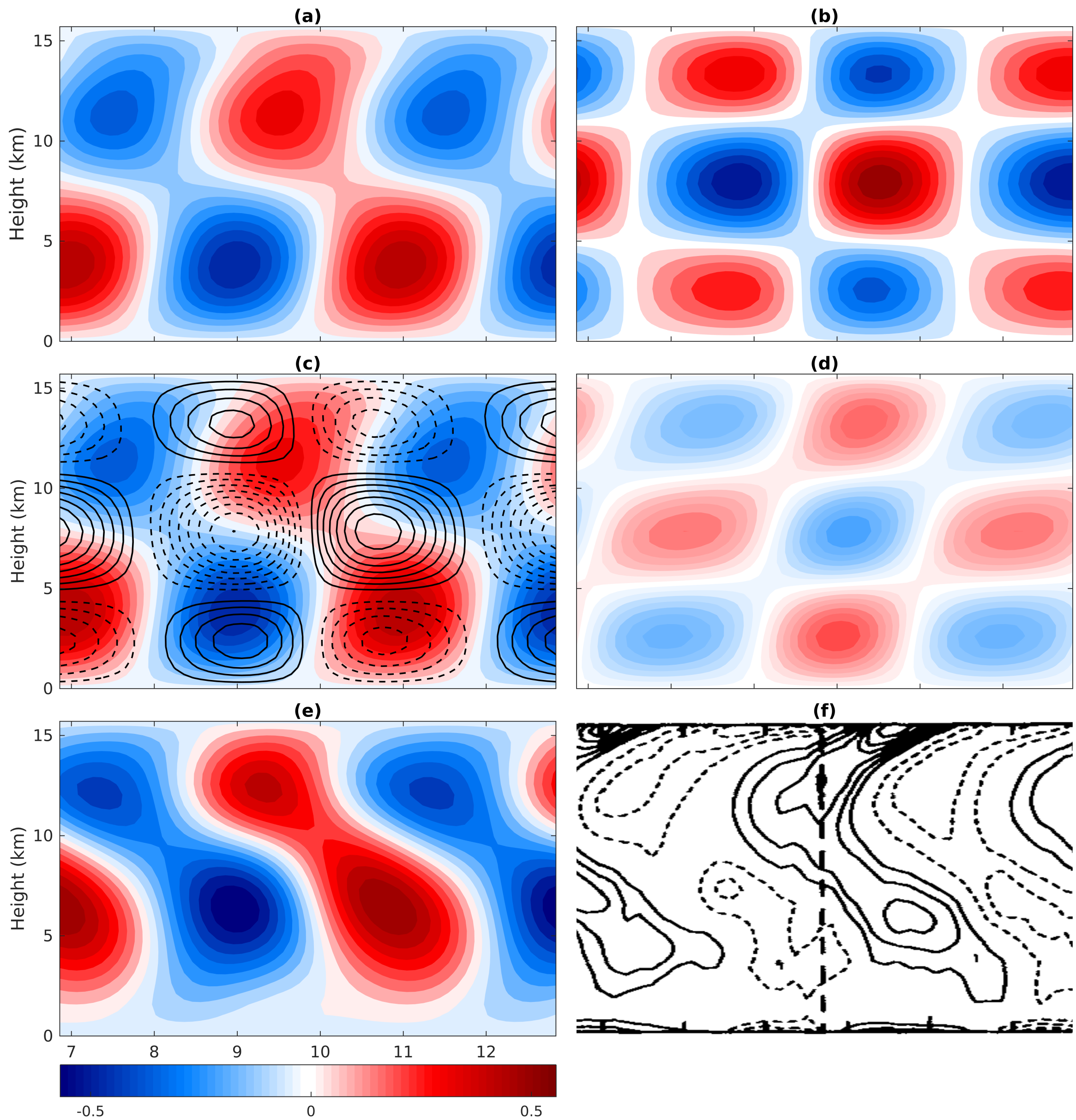


FIG. 6. Potential temperature anomalies (from the domain average at each level) in the longitude-height diagram at 41.5 *day*. The panel (f) shows Figure 13a from the paper (Grabowski and Moncrieff 2001). The rest panels show potential temperature anomalies induced by (a) mean heating, (b) eddy momentum transfer, (c) eddy momentum transfer and eddy heat transfer (contour), (d) eddy heat transfer, (e) total. The contour interval in panel (c) 0.05 $K$ and that in panel (f) is 0.2 $K$. The dimensional unit is $K$.

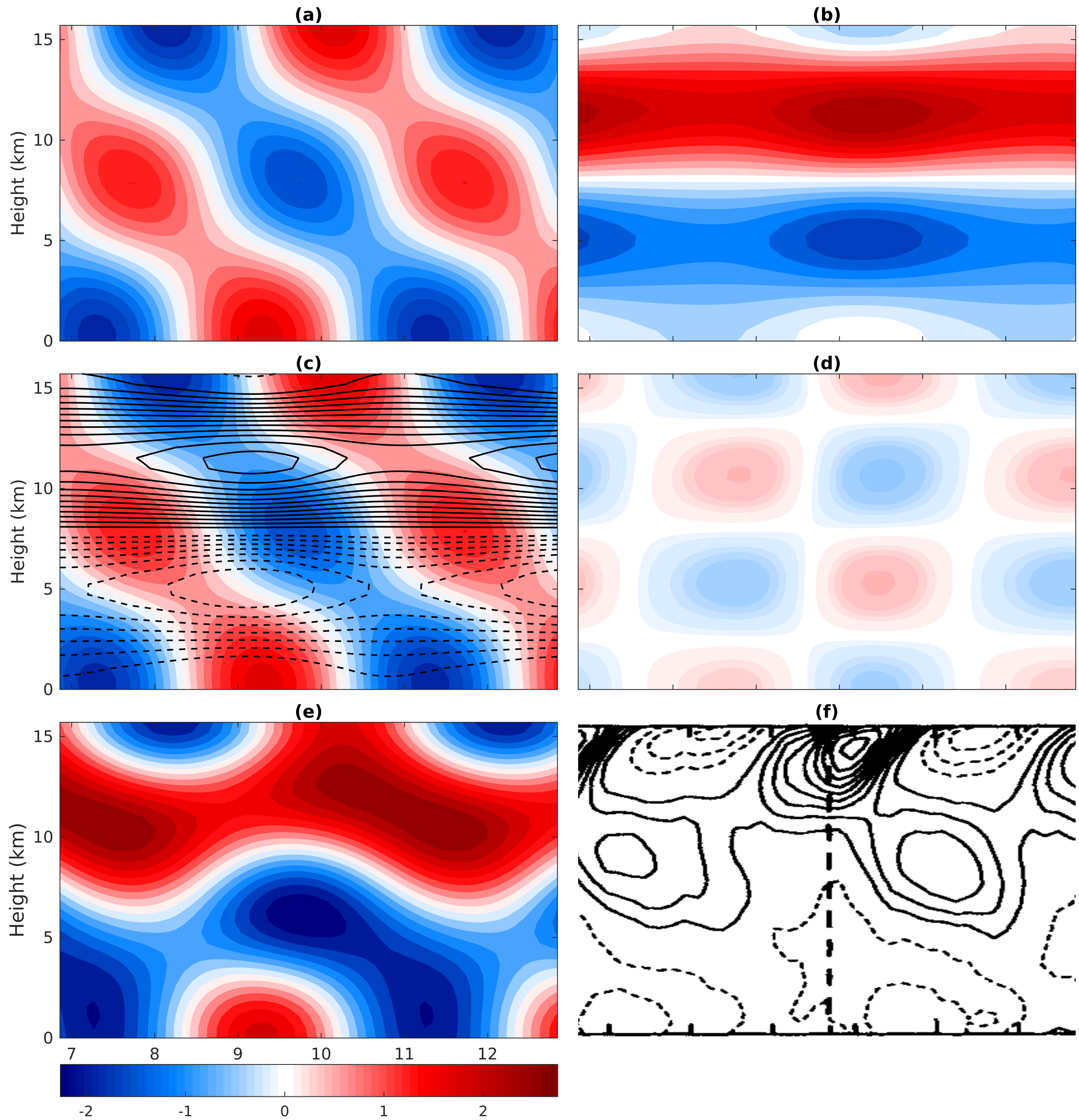


FIG. 7. Zonal velocity in the longitude-height diagram at 41.5 *day*. The panel (f) shows Figure 14a from the paper (Grabowski and Moncrieff 2001). The rest panels show zonal velocity induced by (a) mean heating, (b) eddy momentum transfer, (c) eddy momentum transfer and eddy heat transfer (contour), (d) eddy heat transfer, (e) total. The contour interval in panel (c) is 0.19 $ms^{-1}$ and that in panel (f) is 1 $ms^{-1}$. The dimensional unit is $ms^{-1}$.

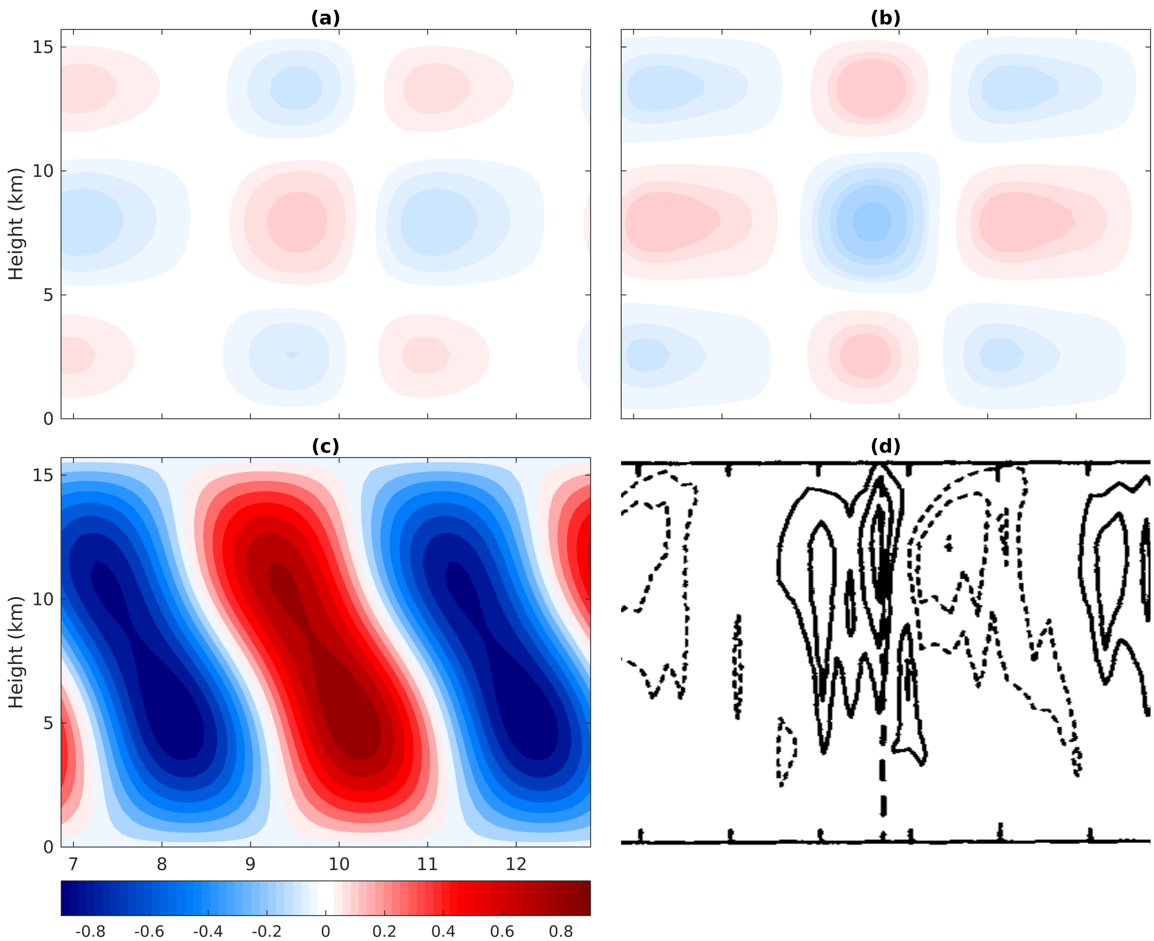


FIG. 8. Vertical velocity in the longitude-height diagram at 41.5 *day*. The panel (d) shows Figure 14b from the paper (Grabowski and Moncrieff 2001). The rest panels show vertical velocity induced by (a) eddy momentum transfer, (b) eddy heat transfer, (c) mean heating. The dimensional unit is $10^{-2}ms^{-1}$. The vertical velocity induced by mean heating in panel (c) has a upward/westward tilt in dominant magnitude, which is different from panel (d). A similar scenario with upright mean heating is discussed in Sec.5.

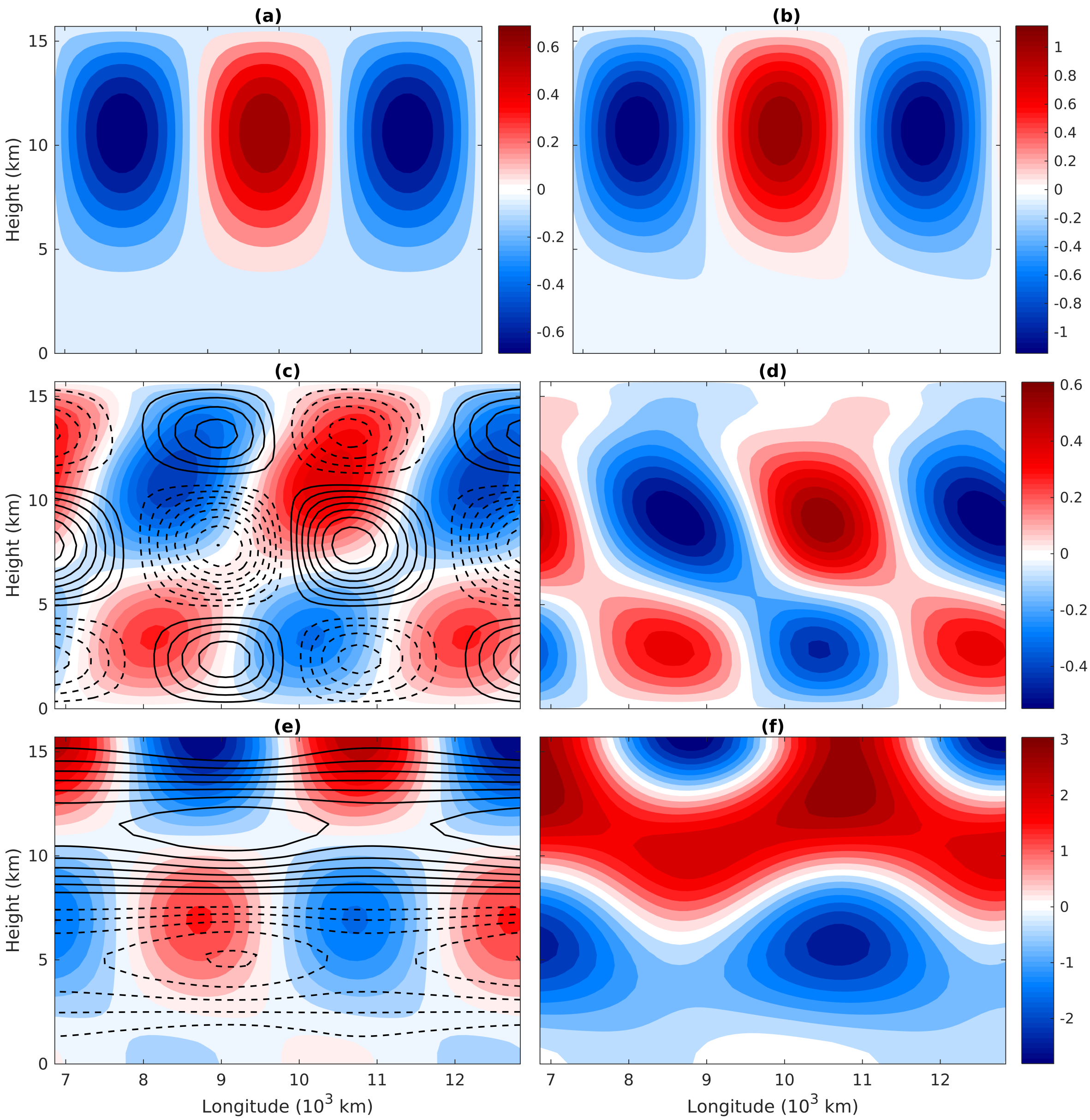


934 FIG. 9. Upright mean heating, potential temperature anomalies (from the domain average at each level), zonal
935 and vertical velocity in the longitude-height diagram at 41.5 *day*. The panels show (a) upright mean heating, (b)
936 vertical velocity, (c) potential temperature anomalies induced by eddy terms (contour) and mean heating (color),
937 (d) total potential temperature anomalies. (e) zonal velocity induced by eddy terms (contour) and mean heating
938 (color), (f) total zonal velocity. The dimensional unit of mean heating, vertical velocity, potential temperature
939 anomalies and zonal velocity are 10 $Kday^{-1}$, $10^{-2}ms^{-1}$, $K$, $ms^{-1}$ respectively.

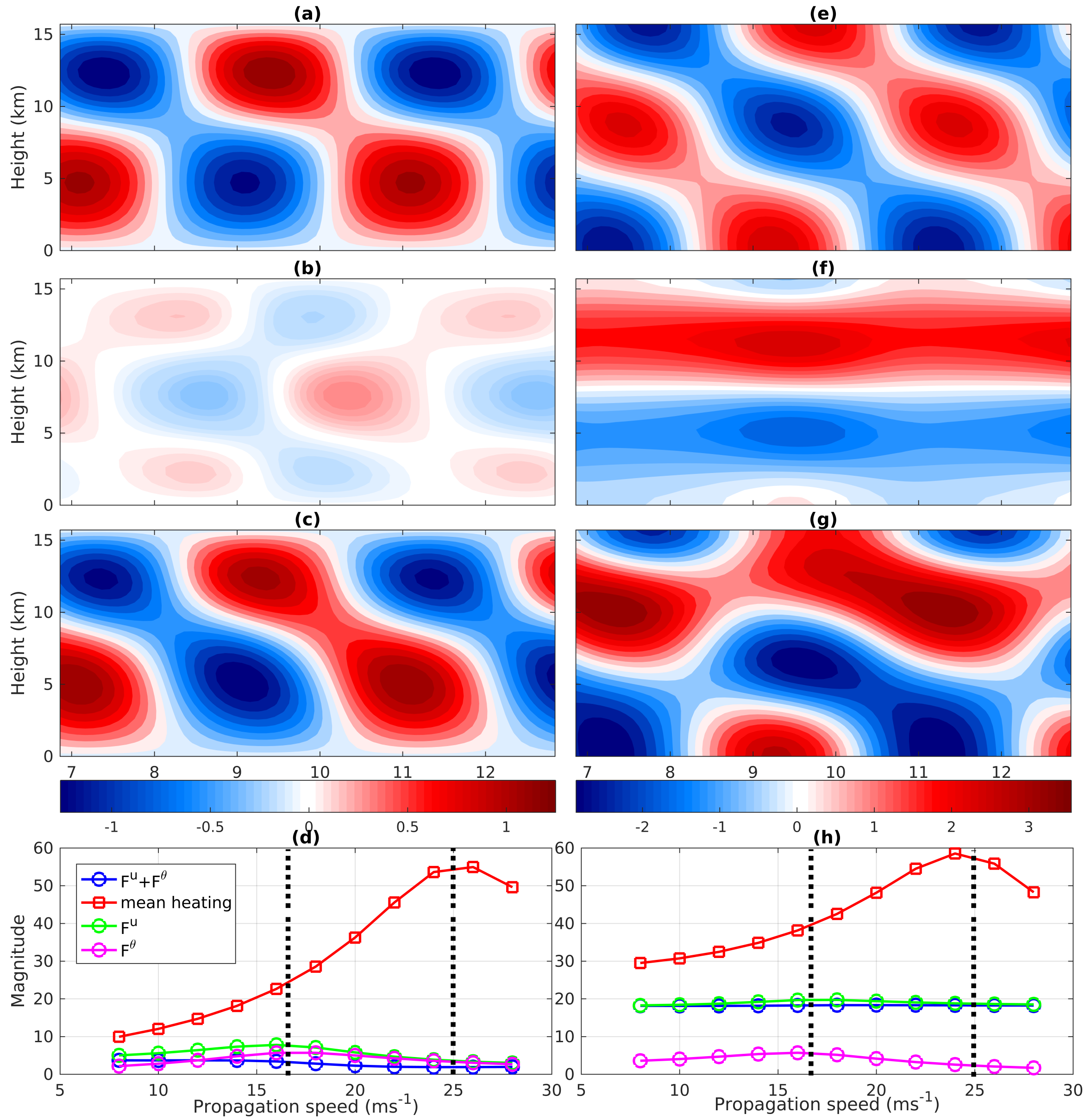


FIG. 10. Potential temperature anomalies (from the domain average at each level) and zonal velocity in the longitude-height diagram at 41.5 *day*. The left panels show potential temperature anomalies induced by (a) mean heating, (b) eddy terms, (c) total. The right panels (d-f) are similar to (a-c) but for zonal velocity. Panel (d) shows potential temperature anomalies in Frobenius norm in different propagation speeds and panel (h) shows the same but for zonal velocity. Panels (d) and (h) share the same legend and the two dashed lines denote the phase speeds of gravity waves in the second (25 $ms^{-1}$) and third (16.7 $ms^{-1}$) baroclinic modes. The dimensional units of potential temperature anomalies and zonal velocity are $K$ and $ms^{-1}$.

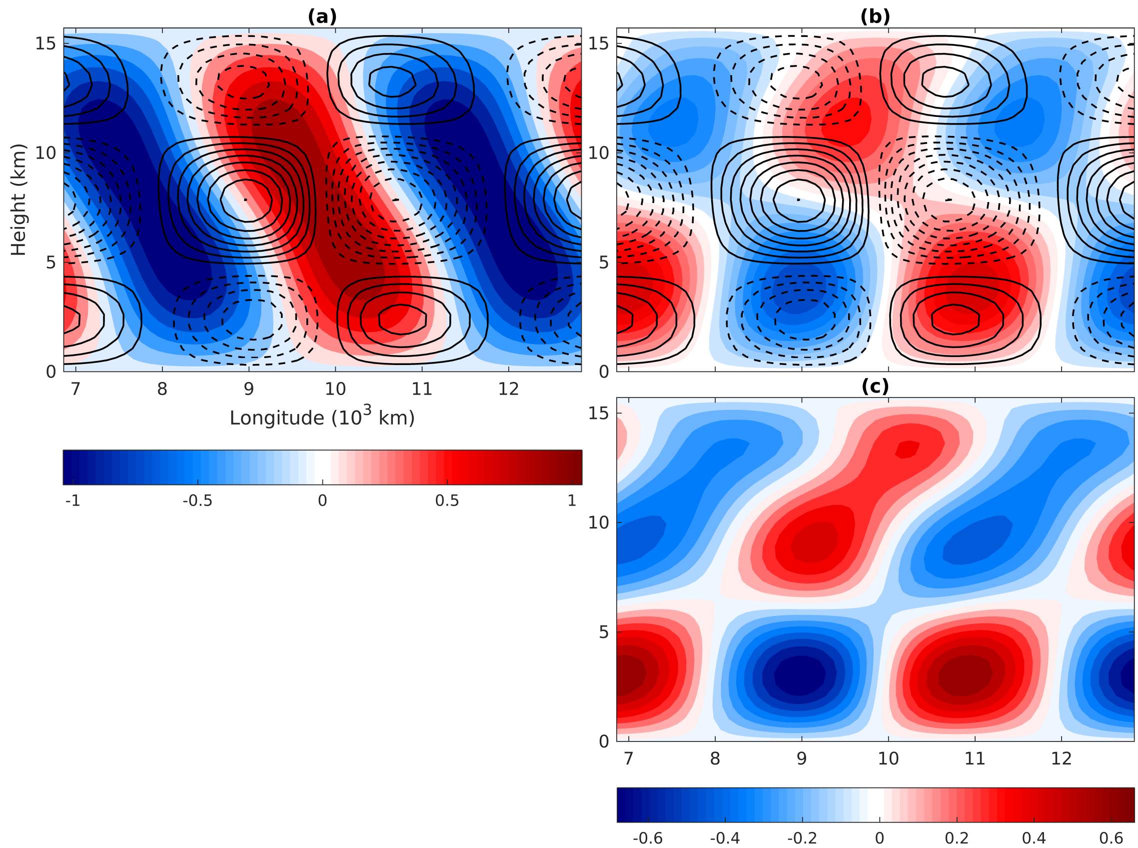


FIG. 11. Potential temperature anomalies (from the domain average at each level) in the longitude-height diagram at 41.5 *day*. Panel (a) shows potential temperature anomalies induced by eddy terms (contour), and mean heating (color). The right panels show potential temperature anomalies induce by (b) mean heating (color) and eddy terms (contour), (c) total. The dimensional units of mean heating and potential temperature anomalies are 10 $Kday^{-1}$, $K$ respectively.